STUDY OF CORRELATION OF DEVICE PARAMETERS WITH DIFFERENT DEVICE STRUCTURES BY VARYING INTERFACE LAYER

A DISSERTATION SUBMITTED TOWARDS THE PARTIAL FULFILLMENT OF

THE REQUIREMENT FOR THE AWARD OF DEGREE OF

MASTER OF TECHNOLOGY

IN

NANOSCIENCE AND TECHNOLOGY

SUBMITTED BY

SUNNY CHUG

(ROLL NO. 2K12/NST/20)

UNDER THE SUPERVISION OF

Dr. SURESH CHAND
(Chief Scientist, NPL, Delhi)

Dr. J.P. TIWARI
(Scientist, NPL, Delhi)

Dr. Mohan S Mehata
(Asst. Professor, DTU, Delhi)

DEPARTMENT OF APPLIED PHYSICS

DELHI TECHNOLOGICAL UNIVERSITY, BAWANA ROAD, DELHI-110042

JUNE -2014

CHAPTER 1

INTRODUCTION AND BRIEF HISTORY OF ORGANIC SOLAR CELL

1.1 INTRODUCTION:

Energy is the single most essential ingredient for sustaining all sorts of life formson earth. Energy makes the lives of billions of people of the world richer, productive and healthier every day. From prehistoric age to the modern era, the energy demand has increased proportionally with the increase in the standard of living and lifestyle of human beings. It is the primary driving force for a country's well-being and prosperity as well as economic growth. According to International Energy Outlook report 2011, the energy demand of the world will increase by 53%, from 505 quadrillion BTU in 2008 to 770 quadrillion BTU in 2035 [1].After the economic downturn of 2008-2009 as the world economy tries to recover, the global energy demand however increases strongly due to strong economic growth and increase in population. The growth in economy for OECD countries rises at the rate of 2% per year whereas for the non-OECD nations, the growth rate is expected to be faster at 4.5% [2].

With the exponential increase in human population the energy demands have increased tremendously and there is no way that we can meet the needs of every human being on earth by solely relying on fossil fuels which unfortunately is the current trend. Moreover, fossil fuels are a non-renewable resource that once depleted would take millions of years to regenerate. With the

current consumption we are heading towards this disaster at amuch faster rate. We need to find other alternatives to meet the increasing energy demands.

Petroleum is the world's number one source of energy, with oil accounting for more than 1/3 of the total energy consumed. In 2007, there was a 30% increase in spending on construction of renewable energy facilities, for a total of $71 billion [3, 4]. Not only are oil and other fossil fuels non-renewable, they contribute to another of the world's scariest problems: climate change. Fossil fuel combustion accounts for 62% of the global warming potential of all anthropogenic greenhouse gases [5].

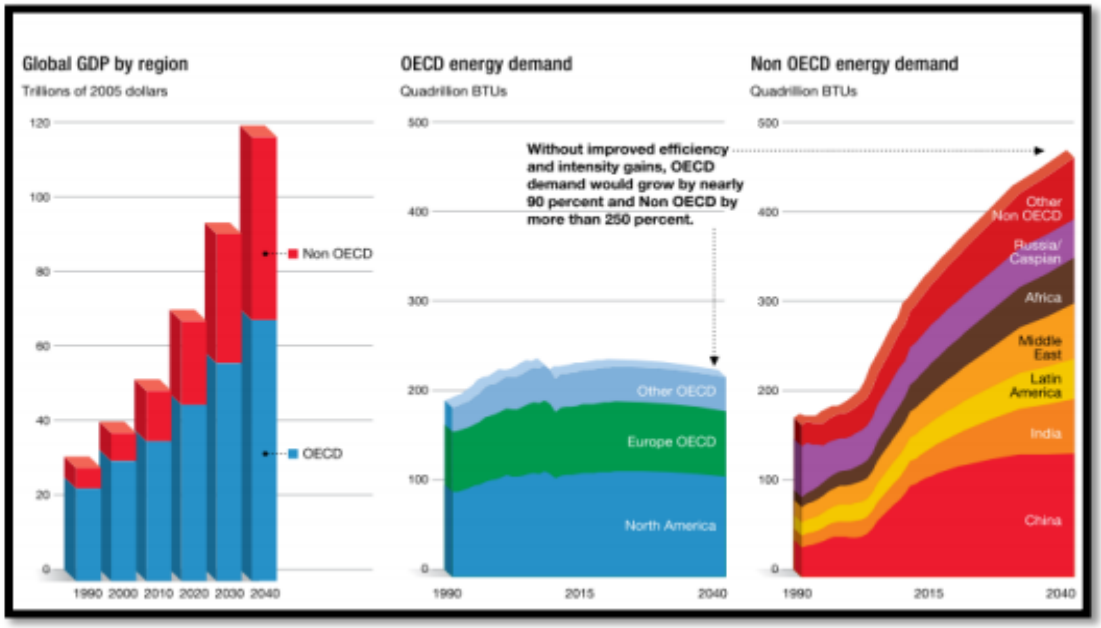

Figure 1.1: Global GDP by region (in trillions of 2005 dollars) (b) Energy demand of OECD nations (in Quadrillion of BTUs). (c) Energy demand of non-OECD nations (in Quadrillion of BTUs) [2].

Another consequence of using fossil fuels is the emission of greenhouse gases. The primary greenhouse gases (GHGs) present in the earth's atmosphere are water vapour, carbon dioxide, methane, nitrous oxide and ozone. These gases trap heat in the atmosphere thus leading to global warming and unwanted climate changes. The burning of fossil fuels has contributed to 40% rise in the concentration of carbon dioxide in the atmosphere from 280 ppm to 400 ppm [7].

Anthropogenic carbon dioxide (CO_2 released due to human activities) come from the combustion of carbon based fuels such as coal, wood, oil and natural gas. In today's world the demand for fossilfuels as described earlier is increasing in proportion to the world population. Development is important but not at the cost of destroying the very world we live in. In a report produced by the Intergovernmental Panel on Climate Change, a panel assembled by the United Nations in 2007, the threat due to greenhouse gases were outlined (GHGs). The anthropogenic greenhouse gas emission along with the global rise in energy demands are one of the pressing issues we face today. These issues need to be resolved at the earliest in order to ensure a bright future for our future generations. Thus, the need of the hour is sustainable development. The need for sustainable development has accelerated research in the areas of renewable sources of energy such as - solar energy. When it comes to renewable sources of energy, solar energy easily takes the lead. Incoming solar radiation intensity is around 1000 W/m^2indicating that roughly 1.5 X 10^7W hits the earth's surface. This is over 500 times the global demand for power. This shows that undoubtedly solar power is going to be one of the prime sources of energy in the coming decades. Thus, the need of the hour is to avoid the over exploitation of these fossil fuels and to rely on renewable sources of energy such as solar energy, wind energy and hydroelectricity to fulfil the energy demands of the coming generations. Solar energy is by far the renewable energy source with the greatest potential (Table 1.1).Here, our focus is on solar energy. Figure 1.2 shows the current and the predicted world energy consumption.

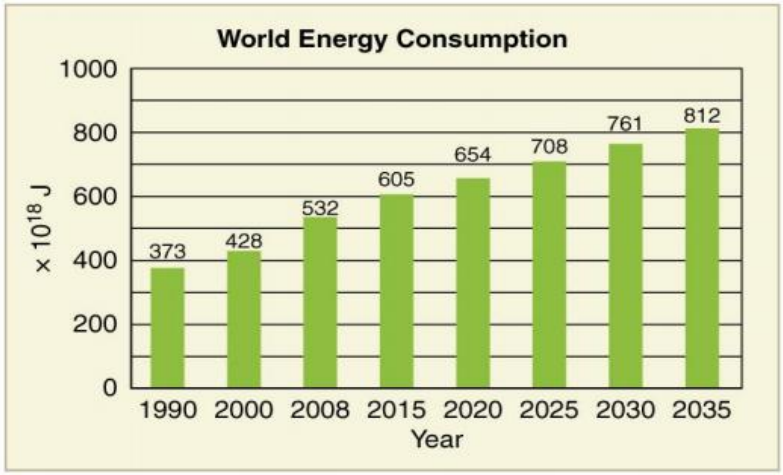

Figure 1.2 World energy consumption [6]

Table 1.1 Energy available for harvesting from different sources compared to the global Energy demand [8]

Global consumption	Hydro	Geothermal	Wind	Solar
15 TW	7. 2 TW	32 TW	870 TW	86,000 TW

1.2 Solar cell :

Photovoltaic industry has grown over 40% over the last decade and it can be majorly attributed to the advancement in silicon based technologies. Cost, sustainability and environmental issues are still the major concern. Competitive technologies have also emerged in the past few decades such as Organic solar cells and dye sensitized solar cells, but low efficiency, lifetime and durability issues make it very difficult for them to challenge the silicon solar cells at least for the next decade or so [9].

Solar cell as we know is a semiconducting device. It converts solar energy into electrical energy (photovoltaic effect). Light which ismade up of packets of energy, called photons, its energy depends on the frequency, or colour, of the light. The solar spectrum covers ultra violet to infrared wavelength ranges. Only 30% of incident light energy is in the visible light range, while over 50% is in the infrared range (Figure 1.3).

The photons in UV and visible range have enough energy to pump electrons in semiconducting material, and this can be effectively used for charge generation. However, IR waves are too weak to generate electricity using conventional PV technology.

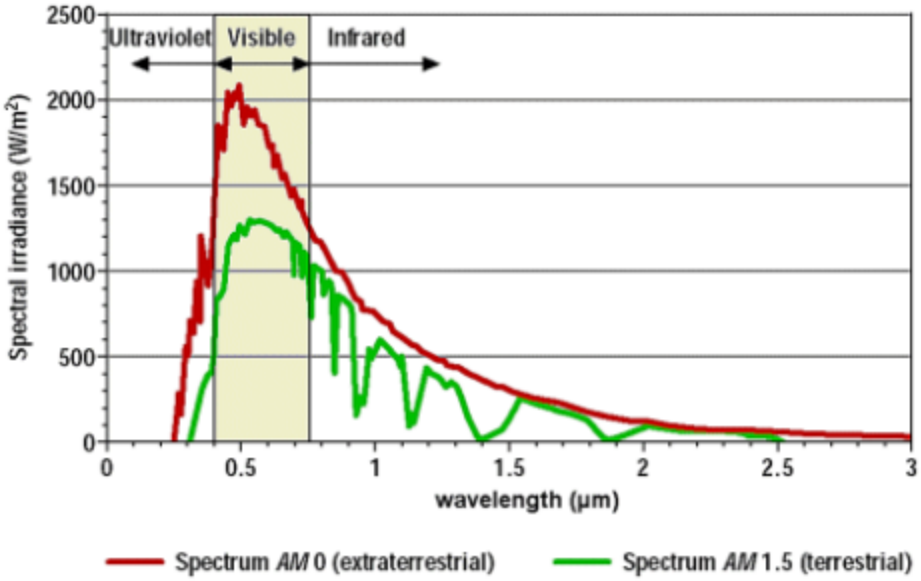

Figure 1.3 Solar Radiation Spectrum

1.3 Generations of Solar Cells:

Solar cells can be best classified in terms of generations i.e. the development and variations in solar cells with time.

So far there have been three such generations of solar cells as follows:

1.3.1 First Generation: -Single PN junction silicon solar cells come under first generation PVs. This category of solar cells is the most commercialized one covering 90 % of the photovoltaic market. [10]. The most important parameter of the performance of a solar cell is its Power conversion efficiency (PCE), i.e. the percentage of incoming solar radiation that is converted to usable power by the solar cell. So far, the highest theoretical efficiency that is reported by Shockley and Queissier i.e. 33% for any type of single cell solar cell with a band gap of 1.1eV [11]. Kerr et al. calculated that for a 90µm thick single j unction solar cell to be 29% [12].

(a) Monocrystalline Silicon Cells: -Solar cells made from thin wafers of silicon are the most prominent solar cell technology currently in spite of being the oldest. These cells are sliced from large single crystals that have been grown in a controlled environment with tremendous efforts and hence called as monocrystalline solar cells. A panel is made up of a number of cells laid out in a grid and are a few inches across (Figure 1.4).They have a higher efficiency (up to 24.2%) as compared to other types of cells which means that more electricity can be produced from a given panel area [12].

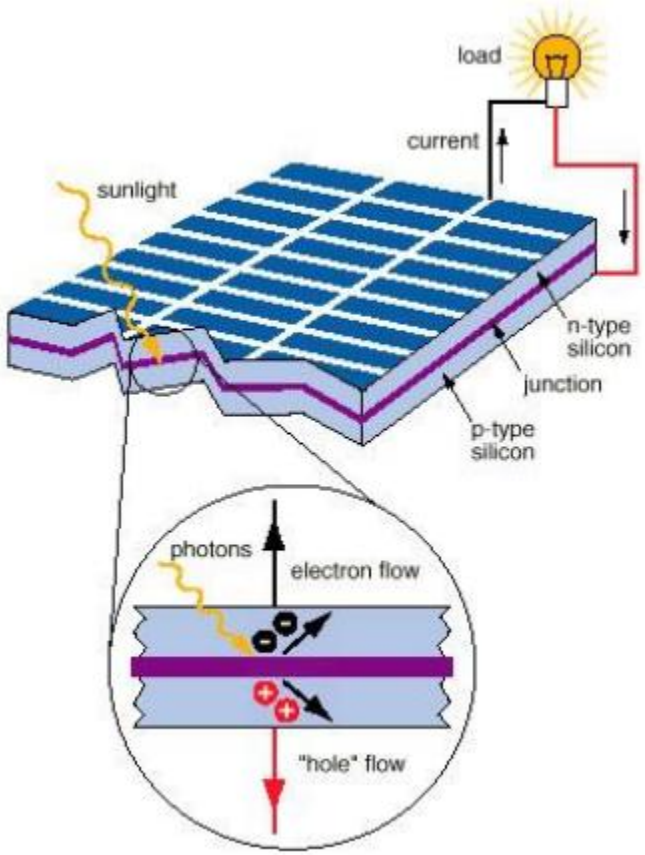

Figure 1.4 A basic schematic diagram for first generation solar cells.

(b) Polycrystalline Silicon Cells -The production of silicon wafers in moulds from multiple silicon crystals rather than from a single crystal is obviously cheaper and easier as compared to the production of monocrystalline solar cells, as the growing environment need not be as controlled and specific. A number of silicon crystals are grown together to make polycrystalline

solar cells. No doubt panels on these cells are cheaper per unit area but they suffer in efficiency (up to 19.3%).

(c) Amorphous Silicon Cells-In amorphous silicon cells of silicon crystals are not grown as is done in the previous two types, instead silicon is deposited in a very sleek layer on a backing substrate such as metal, glass, or plastic. In these cells various silicon layers are mixed with impurities accordingly to respond to various wavelengths of light and are laid in a stack to improve efficiency.

d) Hybrid Silicon Cells-As the name suggests the origin of this type of silicon solar cells was after exploring ways of combining different materials to make a hybrid with better efficiency, stability at reduced costs. Recently introduced hybrid HIT cell consisted of a layer of amorphous silicon over single crystal wafers. It was found that the efficiency improved and even stabilized with fluctuations in temperature of the place. First generation solar cells have highest efficiencies and lifetimes among all other types. The only limitation it faces is its high production cost that prevents them from being economically competitive and hence open doors for other research domains. In August 2010, Solar buzz, an international solar energy research and consulting firm, confirmed the residential price per kilowatt-hour of solar electricity was approximately 35 cents [13].

1.3.2 Second Generation: -The cost related limitations of the first generation solar cells has shifted the focus of the researchers on the development of more cost effective second generation thin film solar cells [14]. The trick behind the reduction in costs of these solar cells lies in the use of less material for their generation. The thin films are only a few micrometers thick which is much less than the crystalline silicon based cells. So use of less material and lower manufacturing costs enables manufacturers to produce and hence sell panels at a comparatively much lower cost. The second generation includes amorphous silicon (mentioned above) and two more that are made up of non-silicon materials – cadmium telluride (CdTe) and copper indium gallium di selenide (CIGS). These solar cells are fabricated by sputtering, physical vapour deposition, and plasma-enhanced chemical vapour deposition. The highest recorded efficiency is as good as 19.6% [14], which is not very far from the crystalline silicon results. This combination of moderately high efficiency and low manufacturing costs makes the second generation solar cells a good area of interest for the researchers.

1.3.3 Third Generation: -This generation marked a completely new era in the development of solar cells giving birth to a totally new direction of research and development, i.e. multijunctioncells, dye-sensitized cells (DSCs), and organicphotovoltaic (OPVs). This approach was also an effort to bring down the costs of solar cells further. Multijunction solar cells aim at maximizingthe efficiency and thereby reducing the relative cost or increasing power to cost ratio. These cells contain multiple cells, with different band gaps, stacked over one another so that they can capture maximum region of solar radiation spectrum. A specific combination of the stack can be made to perfectly match the spectrum and result in the efficiency that can even exceed that reported by Shockley and Queisser. The theoretical efficiency limit has reached up to 66% [15]. The laboratories have already witnessed 40% for triple - junction stacked PVs. In 2008, the National Renewable Energy Laboratory (NREL) reported a world record efficiency for a thin triple-junction gallium indium phosphide and gallium indium arsenide cell to be 41.6% [16] (see Figure 1.4). Organic photovoltaic use polymers for light absorption and even for the PN junction with highest recorded efficiency to be 9.2% [17]. This is not a favorable efficiency however, they can be compensated by their low costs.

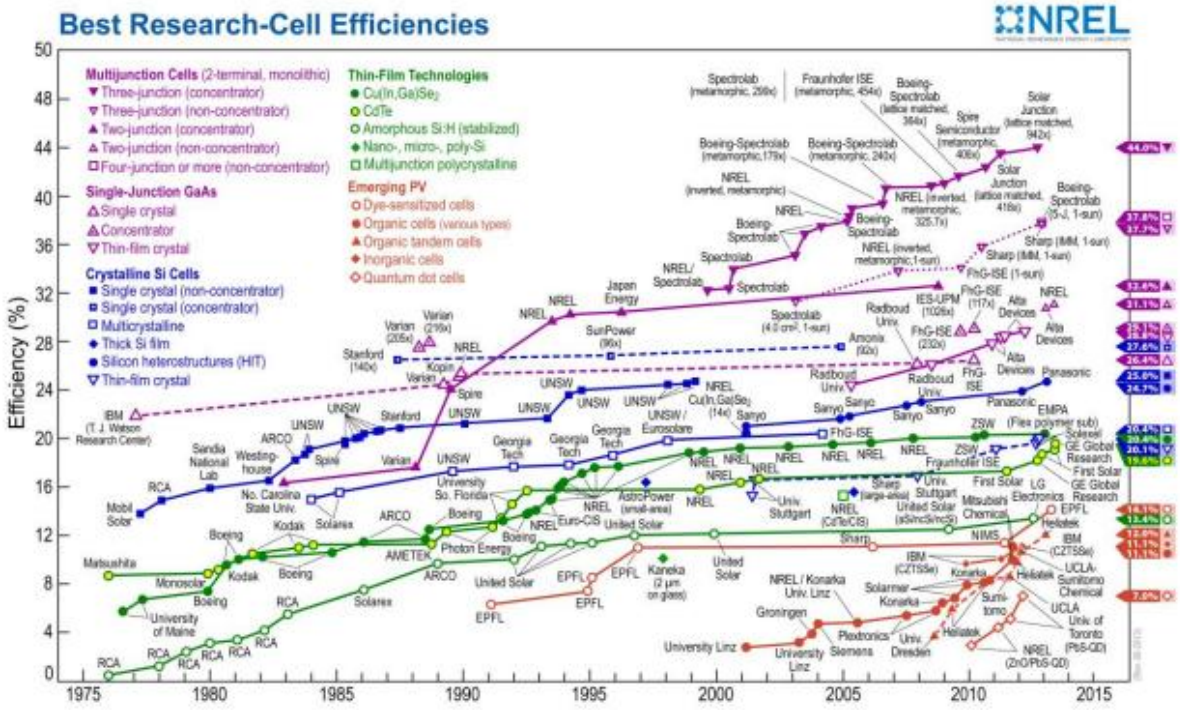

Figure 1.5 The highest recorded efficiencies of a variety of photovoltaic cells [18].

1.4 ORGANIC SOLAR CELL:

1.4.1 Advantages:

Conjugated polymer based solar cells are gaining popularity due to following reasons-

i. Cheap synthesis technique with abundant availability of raw materials.

ii. Possibility to synthesis tailor made molecules with enhanced optical and electrical properties.

iii. Easy processability- Large area, low temperature deposition techniques such as evaporation, ink jet printing makes large scale production possible.

iv. High absorption co-efficient of organic materials makes it possible to absorb the same amount of solar radiation even with nanometer thick films than silicon based solar cells. This makes it possible to make flexible, lightweight solar cells possible.

v. Low manufacturing energy requirements give it an advantage over silicon based counterparts.

vi. Other advantages are low specific weight and high material transparency.

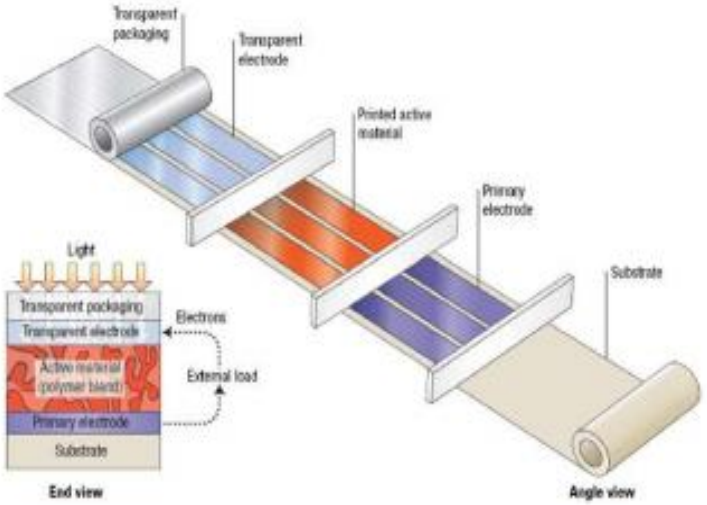

Figure 1.6 Schematic illustration of standard printing processes in polymer solar cells [19].

1.4.2 Different approaches towards OPVs:-

Many different approaches have been successfully employed to produce different types of OPVs.

(a) Dye-sensitized solar cells-First in this category is dye-sensitized solar cell (DSSC) which consists of an organic dye absorbed at the surface of an inorganic wide gap semiconductor. They gained much attention after Brian O'Regan and Michael Grätzel improved the interfacial area between the organic donor and inorganic acceptor using nanoporous titanium dioxide (TiO2). This cell is shown in Figure 1.7.

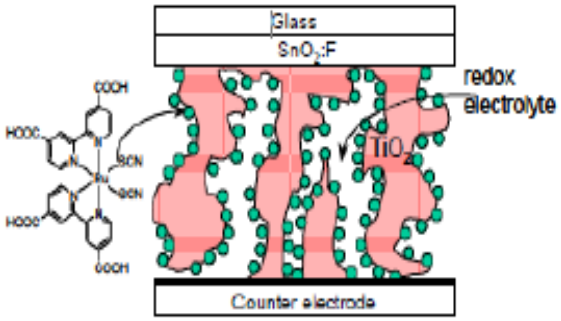

Figure 1.7 Dye-sensitized solar cell

(b) Bilayer Planar heterojunction

In this kind of OSC, donor and acceptor bilayer is used as active layer. Power Conversion Effeciency (PCE) of around 1% was achieved by Tang [20-22] by introducing this concept to the OPV cell in 1979.

(c) Bulk heterojunction (BHJ) cells-

The planar junction concept explained earlier has certain limitations- the need of a long carrier lifetime to ensure that the holes and electrons reach their respective electrodes and a small surface area between the donor-acceptor interfaces. This problem has been addressed by introducing a bulk heterojunction. This involves mixing of donor and acceptor materials in the bulk body of the organic solar cell. In 1995 by the groups of Heeger and Friend independently realized the first efficient heterojunction cell in polymer-fullerene and polymer-polymer blends [23,24].

In these cells, the p-type and n-type layers are combined together forming the p-n junction in the active layer. The greatest concern is that the excitons so generated diffuse to the interface to allow charge separation. But due to their low mobility and short lifetime, the diffusion length is just restricted to ~10nm. Thus for efficient charge generation the distance between the interface and the charge generation site must be of the order of the diffusion length of the exciton. This exciton diffusion is visually depicted in Figure 1.8. Thus, the exciton has to reach a nearest donor-acceptor interface within a few nanometers otherwise it will be lost via recombination thus leading to no charge generation (see Figure 1.8). It was found that even a 20nm thick layer of the active materials was not sufficient enough for efficient photon absorption.

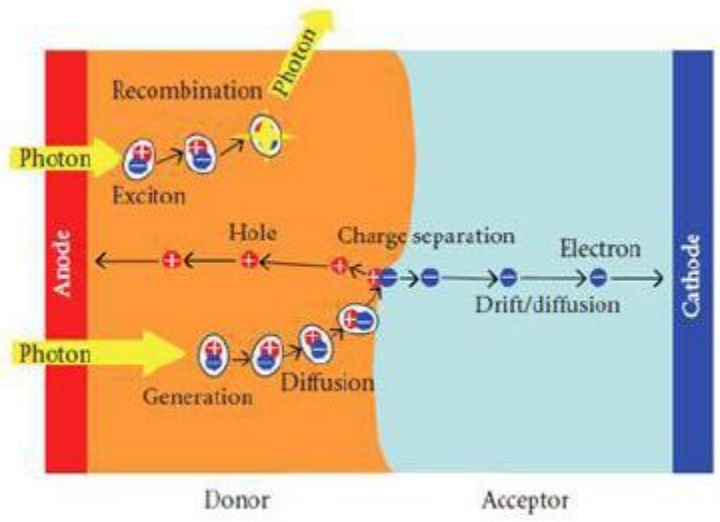

Figure 1.8 Exciton diffusion towards the acceptor-donor interface

So on one hand a thick layer would interrupt the charge separation due to short diffusion lengths of excitons and on the other hand a thin layer would affect the photon absorption. This dilemma was then dealt with a new approach of manufacturing solar cells i.e. by mixing the p and n type materials in the form of a blend and letting the polymers create junctions throughout the bulk of the material, hence ensuring quantitative dissociation of excitons.

The continuous progress in the PCE of BHJ can be observed from Figure 1.5. PCE of bulk heterojunction (BHJ) based polymer solar cells has exceeded 9% [25] in 2012, but it is still much below the value for inorganic solar cells, and in addition, their lifetime is significantly shorter which is major obstacle in their commercialization. However it is predicted that the efficiency of

organic solar cells will cross 12% by 2015 or before (see Figure 1.5) and expected to be commercialized very soon.

In a BHJ solar cell a bi-continuous interpenetration network of the polymer and the acceptor is utilized (Figure 1.10) [25]. A major challenge in this approach was to enable a smooth and effective migration of charge carriers towards their respective electrodes. So, these layers should be mixed into a bi-continuous network in which the inclusions or barrier layers are avoided.

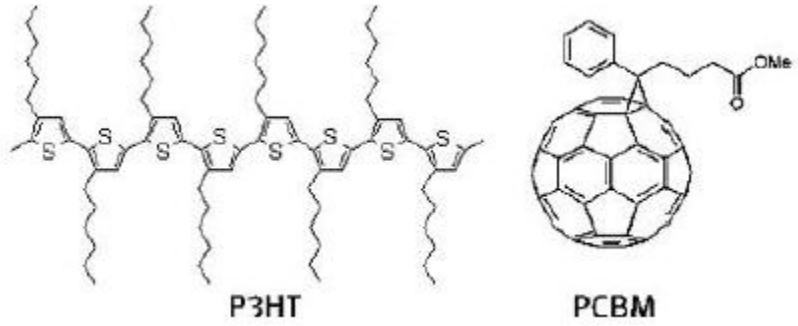

Figure 1.9 The polymer poly (3-hexylthiophene) (P3HT) and the fullerene [6,6]- phenyl-C61 butyric acid methyl ester (PCBM)

In this type, the interface or the heterojunctions are all over the surface or the bulk, hence the name bulk heterojunction.

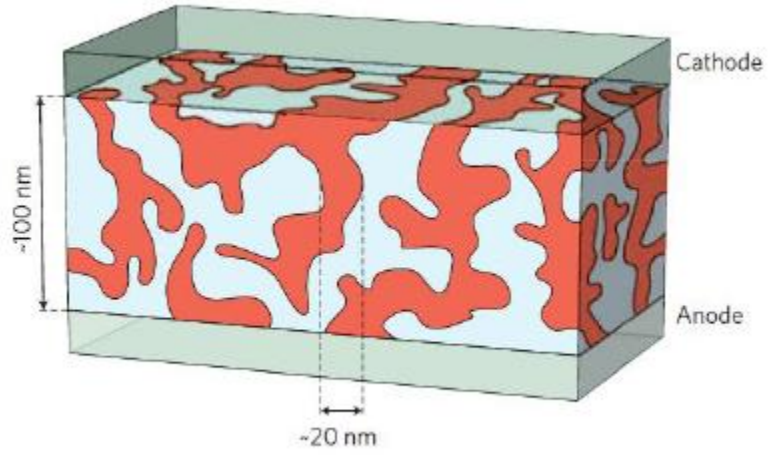

Figure 1.10 Bi-continuous interpenetration network of the polymer and the acceptor [25]

When the photons are incident over the photoactive material, charge transfer occurs due to the mixing of the donor and acceptor material (plane and red area in Figure 1.10). The generated

charges are then transported and collected at the respective electrodes. Even though the BHJ concept is powerful as a solution for addressing the issue of exciton dissociation, in 2005 researchers discovered that the morphology (donor-acceptor phase separation) also plays a important role in achieving good charge transport channels for collecting electrons and holes [26,27].

The role of the photoactive layers with the combination mentioned above is quite overwhelming. At their interfaces there occurs a sub-picosecond charge transfer that leads to efficient charge generation. The lifetimes of the chare separated state extends in these blends hence ensuring an effective diffusion of the generated carriers away from the interface towards the electrodes. This cell is explained in more detail in the organic photovoltaic theory part of this thesis. Our work in this thesis is focussed on study of device parameters using different interfacing layer in BHJ organic solar cell.

1.5 REFERENCES:

[1] U.S. Energy Information Administration, International Energy Outlook, **2011**, report, DOE/EIA-0484**(2011).**

[2] The Outlook for Energy: A View to **2040**, web site: www.exxonmobil.com/energyoutlook.

[3]http://www.bp.com/liveassets/bp_internet/globalbp/globalbp_uk_english/reports_and_publications/statistical_energy_review_2011/STAGING/local_assets/pdf/BP_World_Energy_Outlook_booklet_**2013**.pdf

[4] The Potentials of Renewable Energy**, 2004**

[5] Intergovernmental Panel on -Climate Change, Fourth Assessment Report, **2007**, Working Group III, Chapter 1, p 103

[6] Data from U.S. Energy Information Administration, **2011.**

[7] Justin Gillis, Heat-Trapping Gas Passes Milestone, Raising Fears, **28 May 2013**, the New York Times.

[8] Halls, J. J. M., Cornil, J. dos Santos, D. A., Silbey, R., Hwang, D. H., Holmes, A. B., Brédas, J. L. & Friend, R. H., Charge- and energy-transfer processes at Polymer/polymer interfaces: A joint experimental and theoretical study.Physical Review B, **1999,** 60, 5721.

[9] C.J. Brabec, Organic photovoltaics: technology and market, *Solar Energy Materials and Solar Cells* 83 **(2004)** 273–292.

[10] Frederik C. Krebs. Polymeric Solar Cells: Materials, Design, Manufacture. DEStech Publications, Inc., Lancaster, Pennsylvania, **2010.**

[11] William Shockley and Hans J. Queisser. Detailed balance limit of efficiency of p-n junction solar cells. *Journal of Applied Physics*, **1961**, 32, 510.

[12] M. J. Kerr, A. Cuevas, and P. Campbell, Limiting efficiency of crystalline silicon solar cells due to coulomb-enhanced auger recombination, Progress in Photovoltaics: Research and Applications, **2003**, 11, 97.

[13] Solarbuzz. September URL:http://www.solarbuzz.com/index.asp**, 2010.**

[14] S. E. Shaheen, D. S. Ginley, and G. E. Jabbour. Organic -based photovoltaics: towards low cost power generation. MRS Bulletin**, January 2006**, 30, 10.

[15] M. LoCascio. Application of semiconductor nanocrystals to photovoltaic energy conversion devices.Evident Technologies, Troy, NY, **2002** (August).

[16] M. A. Green, K. Emery, Y. Hishikawa, and W. Warta, Solar cell efficiency tables (version 36), Progress in Photovoltaic: Research and Applications, **2010**, 18, 346.

[17]Zhicai He, ChengmeiZhong, Shijian Su, Miao Xu, Hongbin Wu and Yong Cao, *Nature Photonics*, **2012**, 6, 591.

[18] Lawrence Kazmersk. Best research solar cells efficiencies. NREL, **2010**

[19]R.Gaudiana, C.J.Brabec, Organic materials-fantastic plastic, *Nature Photonics*,

2008, 2, 287.

[20]Tang, C. W. Multilayer organic photovoltaic elements, *US patent 4*, **1979**, 164, 431.

[21]Tang, C. W. 2-layer organic photovoltaic cell, *Appl. Phys. Lett.*, **1986**, 48, 183.

[22]Gang Li, Rui Zhu and Yang Yang, Polymer solar cells, *Nature Photonics*, **2012**, 6, 153.

[23]Yu, G., Gao, J., Hummelen, J. C., Wudl, F. &Heeger, A. J. Polymer photovoltaic cells — enhanced efficiencies via a network of internal donor–acceptor heterojunctions, *Science*, **1995**, 270, 1789.

[24]Halls, J. J. M. et al. Efficient photodiodes from interpenetrating polymer networks. *Nature*, **1995**, 376, 498.

[25]Gang Li, Rui Zhu and Yang Yang, Polymer solar cells, *Nature Photonics*, **2012**, 6, 153.

[26]Li, G. et al. High-efficiency solution processable polymer photovoltaic cells by self-organization of polymer blends, *Nature Mater.*, **2005**, 4, 864.

[27]Ma, W. L., Yang, C. Y., Gong, X., Lee, K. &Heeger, A. J. Thermally stable, efficient polymer solar cells with nanoscale control of the interpenetrating network morphology, *Adv. Funct. Mater.*,**2005**, 15, 1617.

CHAPTER 2

BASIC PRINCIPLE OF ORGANIC SOLAR CELL

2.1 Inorganic Photovoltaic Theory:

In inorganic photovoltaic, a p-n junction is responsible for free charge generation on the arrival of photons from the external light source. A p -n junction is a simple interface between a p type (excess holes) and n type (excess electrons) semiconductor (see Figure 2.1). A p type semiconductor can be formed by diffusing boron (three valance electrons) into silicon. This causes the generation of positive (hole) carriers throughout the lattice. N type semiconductor can be formed by doping phosphorous into the silicon wafer. This doping causes generation of excess electrons in the silicon lattice.

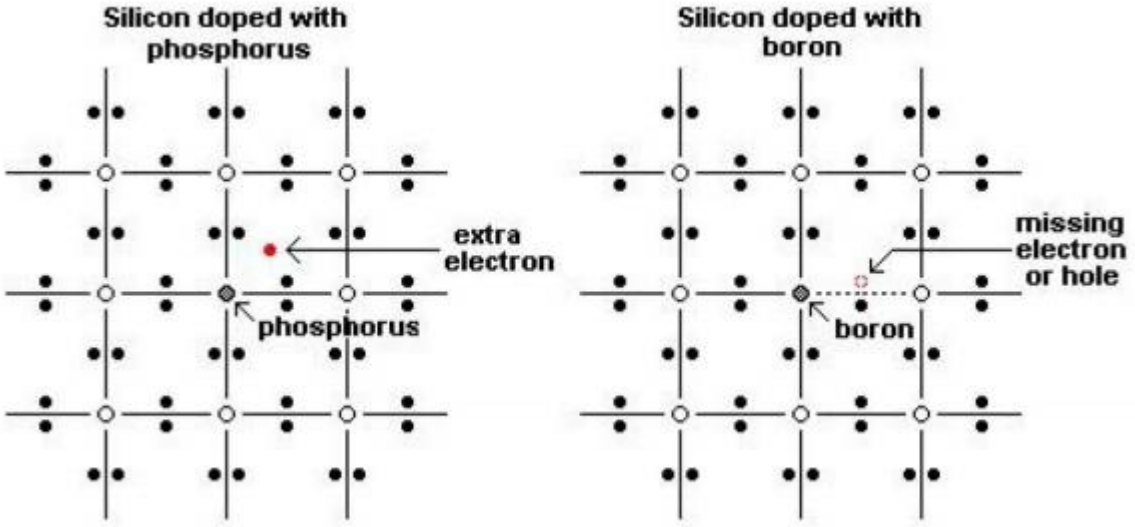

Figure 2.1 From left to right: n and p-type doping of silicon wafer

When an N-type and P-type material are kept together to form a junction, the electrons from the N-type diffuse into the P-type and the holes from the P-type diffuse into the N-type. Thus, positive ions are left behind in the N -side and negative ions in the P-side. This region is devoid of any free charge carriers (electrons and holes). This region is called the depletion region. This process can be visually depicted as shown in Figure 2.2. Valence electrons in Si absorb the incoming photons from an external light source. Photons with adequate energy excite the electrons across the forbidden gap into the conduction band. Thus, these electrons being free in nature can be channeled through an external circuit producing current.

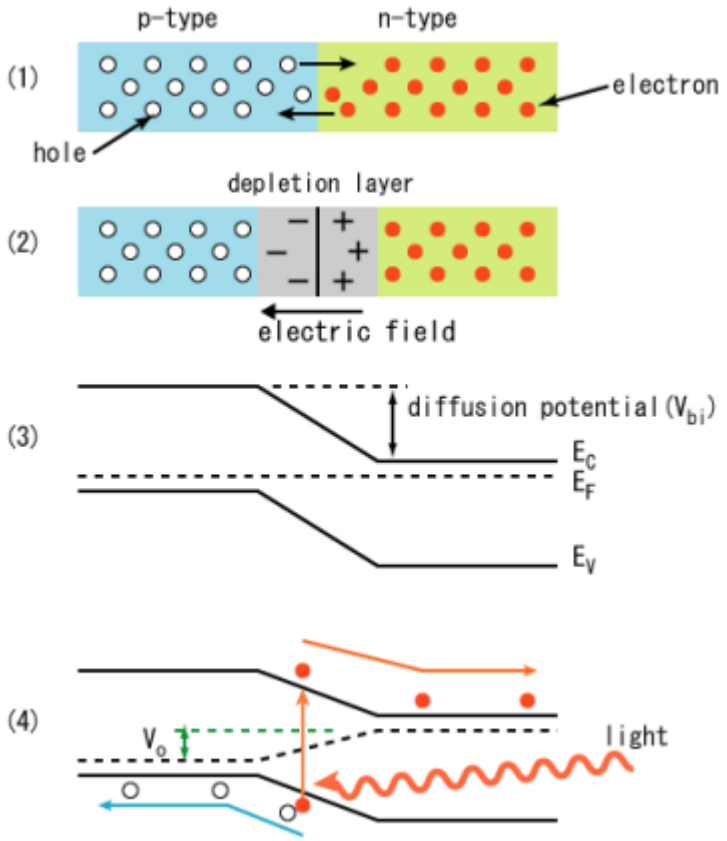

Figure 2.2 The pn-junction of an inorganic solar cell (open circuit); 1) electrons close to the junction, or boundary, diffuse into the p-type region; 2) charge builds up along the interface of the two materials, creating an electric field that opposes the flow of electrons; 3) the conduction and valence bands; 4) a photon excites an electron into the conduction band, and the electron and its positive hole are forced to opposite ends of the cell by the intrinsic electric field.

2.2 Organic Photovoltaic Theory:

At first glance it looks as the organic photovoltaic cells work similar to inorganic photovoltaic cells but on closer inspection we notice that there are significant differences between the two photo-conversion mechanisms. Here in organic photovoltaic, absorption of photons leads to exciton generation. An exciton is a bound state of an electron and hole which are attracted to each other by the electrostatic Coulomb force. PV cell structures based on organic materials differ from that based on inorganic materials. Inorganic semiconductors generally have a high dielectric constant and a low exciton binding energy (E.g. GaAs, BE= 4meV). Thus, at room temperature thermal energy being $k_BT = 0.025eV$, the excitons generated due to the absorption of a photon dissociate themselves into positive and negative charge carriers. These charge carriers are easily transported due to the existing p-n junction field and the high mobility of the charge carriers. Contrary to that in inorganic materials, in organic materials the dielectric constant is higher along with the exciton binding energies. The exact magnitudes of binding energies still remain a matter for debate. For polydiacetylene 0.5eV is required to split the exciton and thus dissociation of excitons does not occur at room temperature. To overcome this exact problem organic solar cells utilize two different materials that differ in the electron accepting and electron donating properties. Charges can then be created by photo induced electron transfer between the two components in the solar cell.

2.3 Basic Processes in an Organic Solar Cell:

When it comes to the working of an organic solar cell (OSC), four basic processes or events can be outlined:

1. Absorption of light
2. Charge transfer and separation of the opposite charges
3. Charge transport
4. Charge collection

The above four processes (in the order mentioned) are responsible for the working of an OSC. Care should be taken that for an efficient collection of photons, the absorption spectrum of the active material in the organic solar cell should match the solar emission spectrum.

Charges are created during the photo-induced electron transfer. Here, the electron is transferred from an electron donor (D) a p-type semiconductor to an electron acceptor (A) an n-type semiconductor with the aid of photons (hυ):

$D + A + h\upsilon \rightarrow D^* + A$ (or $D + A^*) \rightarrow D^{\bullet+} + A^{\bullet-}$

After the excitation of the donor (D) or the acceptor (A), charge separated states consisting of the radical cation of the donor ($D^{\bullet+}$) and the radical cation of the acceptor ($A^{\bullet-}$) are created. Also, another important point is that for efficient charge generation, the charge separated state should be the thermodynamically and kinetically most favourite pathway after photo-excitation. Therefore, the photon energy should be used for generation of the charge separated state and is not lost via some other process such as fluorescence or non-radiative decay. The photovoltage (or open -circuit voltage, VOC) is directly linked to the energy difference between the LUMO level of the acceptor and the HOMO level of the donor, thereby providing the primary driving force for charge separation[1].

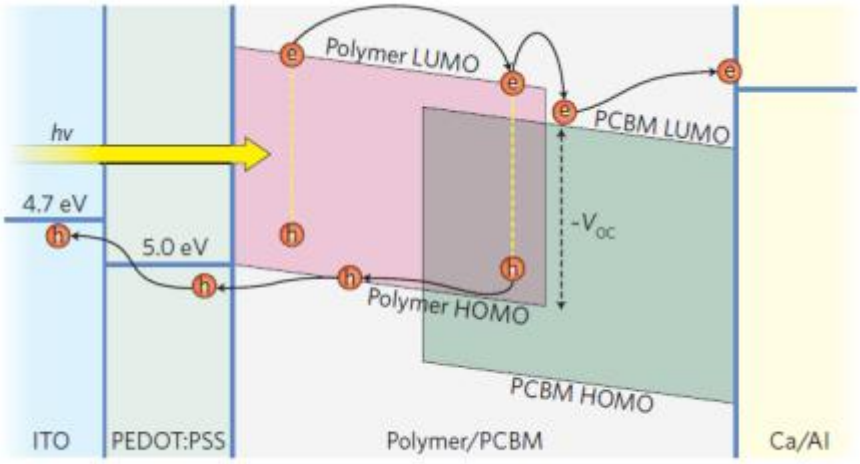

Figure 2.3 Photo-excitation of electrons in donor and the transfer of the electrons into the acceptor; Adapted from [1]

Due to photo-excitation, the electron in the donor moves from the highest occupied molecular orbital (HOMO) to the lowest unoccupied molecular orbital (LUMO) of the donor. This has been shown in Figure 2.3 where ITO is taken as the front electrode with PEDOT: PSS as the buffer layer (or interlayer) and Al as the metallic back electrode. Consecutively, the electron moves to the LUMO of the acceptor thus creating the charge separated states - A▪-and D▪+. These photo-generated charges are then collected at the opposite electrodes. Similar process can occur when the acceptor is excited instead of the donor material. The donor and the acceptor materials are sandwiched between two dissimilar electrodes, one being a transparent electrode (ITO) and the other a metallic electrode. The structure of organic solar cells is explained in more detail in the next section (Sec. 2.4) of this chapter.

As explained in the previous chapter, among the various approaches to make organic solar cells, bulk heterojunction cells prove to be one amongst the best performing solar cells to due to the many interfaces formed (between the p -type and n -type materials) in the cell. We have focused our research on bulk heterojunction cells.

2.4 Structure of a BHJ:

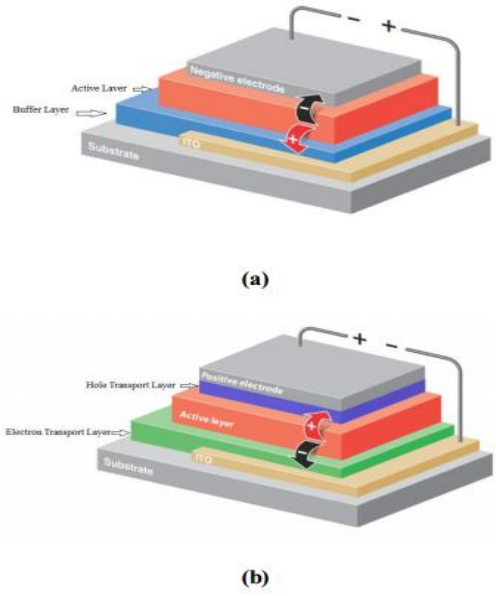

Figure 2.4 Structure and geometry of bulk heterojunction solar cells a) Normal (Conventional) Cell b) Inverted cell

2.4.1 Geometry of Organic Solar Cell:

We have two different geometries- normal (or conventional) cell and inverted cell. In a normal cell electrons move towards the metallic electrode which has a lower work function compared to indium tin oxide (ITO) making this electrode as cathode. Whereas, in an inverted cell electrons move towards ITO. Here ITO functions as the cathode. These two geometries are depicted in Figure 2.4.

Both the geometries have their pros and cons of using them. The normal cell features higher efficiencies (recently even inverted cells are known to be highly efficient). The inverted cell being highly stable and can even last for months without much degradation. Inverted devices apart from being more stable are also now as efficient as conventional devices. In inverted devices the electrodes are interchanged i.e. ITO becomes the cathode and the metallic electrode becomes the anode. In these devices, electrons flow towards ITO and holes move towards the metallic back electrode.

2.4.2 Active Layer:

The active layer is where the interfaces between the p -type and n -type materials are made. Here the excitons are generated on photo -excitation. These excitons generated, diffuse into the interface where charge separation occurs. This distance to the interface must be shorter than the exciton diffusion length. In case the exciton length is insufficient, the exciton loses all its energy i.e. recombination occurs even before it reaches the interface. Thus, no charge separation is able to occur in this scenario. Due to low mobility and short lifetime in case of single exciton diffusion, the diffusion length in organic semiconductors is about 8.0 ± 0.3 nm [2].

So, as stated above the active layer is comprised of two materials - p-type and n -type materials. Due to their intrinsic tendency to phase separate on the Nano -scale, junctions (or interfaces) throughout the bulk of the layer are created.

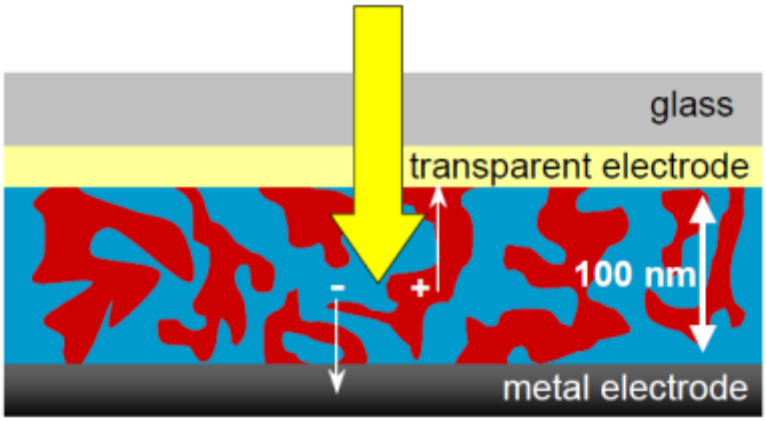

Figure 2.5 Diagram depicting the junctions present in the active layer [3]

To prepare the active layer, the donor and the acceptor materials are mixed in a particular weight ratio. Once mixed in the proper solvent, the prepared solution is allowed to stir for many hours. These materials should be mixed into a bi -continuous, interpenetrating network for the proper formation of junctions and pathways for exciton diffusion. See Figure 2.5. This kind of bulk heterojunction was first explained by Yu et al. in 1995 [4].

2.4.3 Electrodes:

Every organic solar cell consists of two electrodes - the front electrode and the back electrode. In case of normal (or conventional) structure, the front electrode collects holes and the back electrode needs to have a higher work function. In case of inverted structure, the front electrode collects electrons. Here, the back electrode needs to have a lower work function compared to the front electrode.

ITO is used as the transparent front electrode. The front of the cell needs to be transparent in order allow maximum light to reach the active layer. CVD (chemical vapour deposition) graphene is a suitable alternative to ITO. The work functions of ITO and grapheme are 4.8eV [5] and 4.5 eV [6]. They have mid-range work functions and thus can serve as either anode or cathode. Al has a low work function (4.1 eV [2]) and is generally used as the cathode. Certain thin interlayers such as Ca, CsF, or LiF (~1nm) film thermally evaporated on Al are known to provide better performance [7]. Apart from these layers having a lower work function, they also act as a protective layer between aluminium and the active layer.

2.4.4 Intermediate Layers and device structures:

The contribution of intermediate layers in OPVs is enormous. In the conventional structure of organic solar cells usually PEDOT: PSS or poly (3,4ethylenedioxythiophene) poly (styrenesulfonate), a conjugated polymer, is used as a hole conducting layer between the active layer and ITO (Figure 2.6) [8]

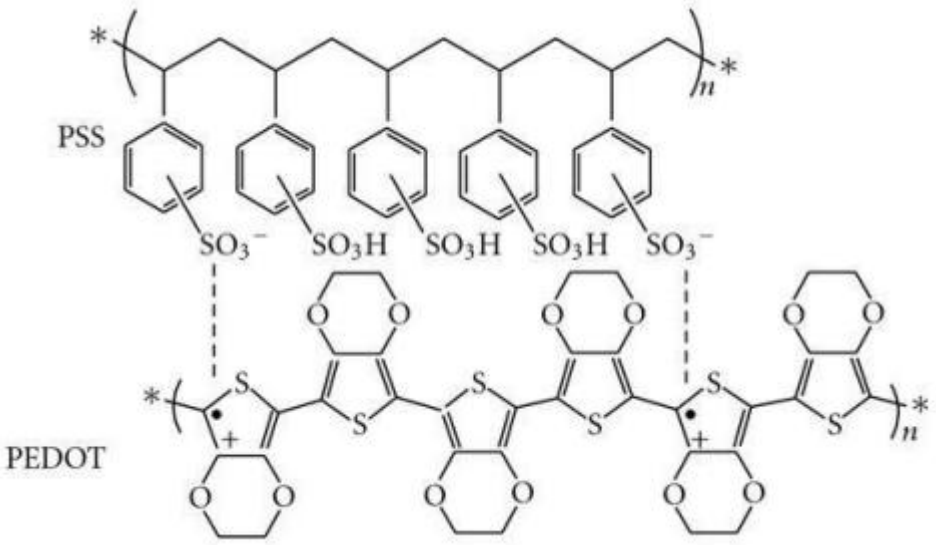

Figure 2.6 The chemical structure of poly (3,4-ethylenedioxythiophene)

poly (styrenesulfonate) (PEDOT: PSS) [9]

Electron conducting layers include zinc or titanium dioxide nanoparticles. Based on the structure of the device we determine whether a hole conducting layer is required or an electron conducting layer. Different intermediate layers can be seen for conventional and inverted structures of organic solar cells in Figure 2.4.

Intermediate layers perform many functions. They permit a single type of charge to pass thus, blocking the opposite charges, and hence prevent recombination i.e. an electron transport layer would act as a hole blocking layer and vice -versa.

The intermediate layers may act as steps for electrons or holes as they move from the active layer to the electrodes with unaligned energy levels. Also, these layers on top of the rough ITO, prevent shunts and does not allow any alternative paths for current to pass [10]. The ITO is made

rough for maximum photon scattering. It is well known that the electrical properties of intermediate layers are very important for the performance of the devices as they will affect charge transport at the interface. The conductivity of wide bandgap metal oxides (e.g., ZnO and TiO2) are sensitive to UV light [11-14].

In our investigation, we are using new ZnO-polymer such as ZnO-PDADMAC nanocomposites and PFN as electron transport (or conducting) layers. These layers offer better device performance when used as ETL compared to pure ZnO film.

Table 2.1 Different materials used in conventional and inverted device structures

Cell Structure	**ETL**	**HTL**	**Anode**	**Cathode**
Conventional	Ca,CsF,LiF	PEDOT:PSS	ITO	Al, Ag, Au
Inverted	ZnO, TiO_2	MoO_3	Al, Ag, Au	ITO

2.5 Motivation:

Interface layers have various functions in BHJ cells such as:

(1) They are able to reduce energy barrier between active layer and electrodes and can promote the formation of ohmic contacts for effective charge collection

(2) They can form selective contacts for charge carriers.

(3) They can modify the electrode work function and can change conventional structure to inverted structure.

(4) They can protect active layer and can modify the field inside.

Generally, PEDOT:PSS is applied on top of ITO to form the ohmic contact for the effective charge collection but acidic nature of PEDOT:PSS creates problems and researchers have tried

various metal oxides such as MoO_3, V_2O_5, WO_3 and NiO. However, solution processed metal oxide has become popular these days due to their low cost deposition.

Recently n-type inorganic metal oxides such as- ZnO have been shown to be good candidates for interface layers in OSCs. Further, the materials with permanent dipole moments can also be used to modify polymer-electrode interfaces. The work function can be increased or decreased by employing polymer layers in view of their electron withdrawing and electron donating properties. By controlling the dipole moment of polymer layers, one can improve efficiency of BHJ using ZnO combined with polyelectrolytes. Polyelectrolytes maybe other successful candidates for the modification of the polymer-electrode interface. In view of above said observations we also motivated to work on the replacement of interface layer by a combination of ZnO and polyelectrolyte based nanocomposite(PDADMAC). Further, we also replace ZnO nanocomposite with PFN layer to analyze the different device parameters

2.6 Characterization:

Characterization of solar cells is carried out by measuring the current against different values of voltage across the cell. An ideal solar cell resembles a diode connected in parallel with a current source. When no light is incident on the cell, the I V characteristics of the cell resemble to that of a diode. Most of the information can be deducted from the IV characteristics under dark as well as light conditions.

On light absorption, current is generated in the device. The power generated is given by,

$$P = VI, \tag{1}$$

Where I is the current and V is the voltage, maxim power generated can be calculated from the I V curve.

Power conversion efficiency (PCE) (η) can be calculated using the relation,

$$\eta = \frac{I_{sc} \times V_{oc} \times \mathrm{FF}}{P_{light}} \tag{2}$$

Fill factor (FF) is also an essential parameter in determining the solar cell performance. It is the ratio of maximum measured power to maximum theoretical power. Fill factor (FF) is given by

$$FF = \frac{I_{max} V_{max}}{I_{SC} V_{OC}} \tag{3}$$

Where, I_{SC} is the short circuit current i.e. the current when voltage equals zero and V_{OC} is the open circuit voltage i.e. the voltage when current equals zero.

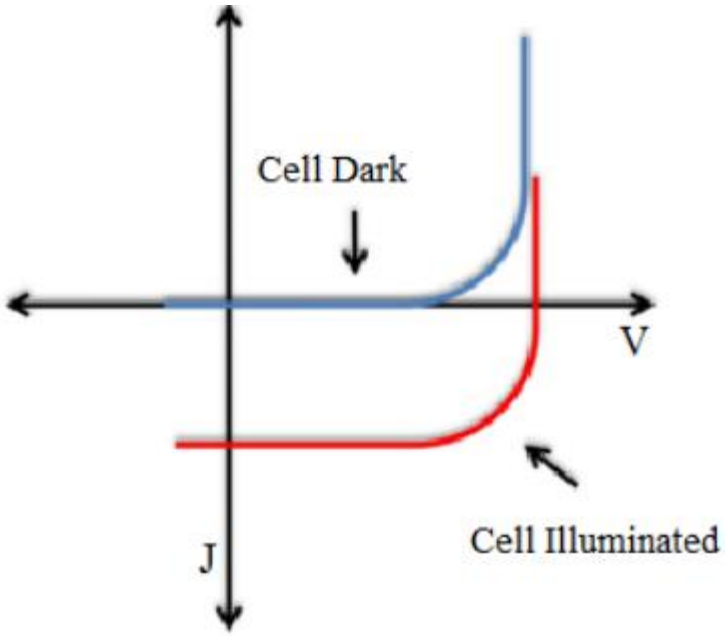

Figure 2.7 J-V curves of an illuminated and dark solar cell; adapted from [38]

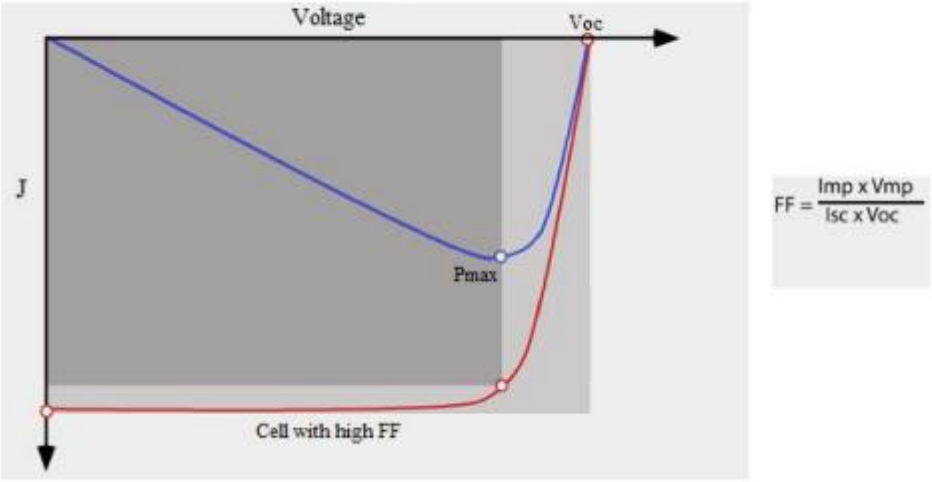

Figure 2.8 Visual illustration of fill factor (FF); adapted from [39].

In order to simplify the internal working of the solar cell, the cell can be modelled into an equivalent circuit consisting of a diode connected in parallel with a current source along with series and shunt resistance which is explained in chapter 4 in detail.

2.7 References:

[1] Gang Li, Rui Zhu and Yang Yang, Polymer solar cells, *Nature Photonics*, **2012**, 6, 153.

[2] Richard R. Lunt, Noel C. Giebink, Anna A. Belak, Jay B. Benziger, and Stephen R. Forrest, Exciton diffusion lengths of organic semiconductor thin films measured by spectrally resolved photoluminescence quenching, *Jol. Of Applied Physics***, 2009,** 105, 053711.

[3] Introduction to polymer solar cells, René Janssen, Departments of Chemical Engineering & Chemistry and Applied Physics Eindhoven University of Technology, The Netherlands.

[4] G. Yu, J. Gao, J.C. Hummelen, F.Wudl, and A.J. Heeger. Polymer photovoltaic cells enhanced efficiencies via a network of internal donor -acceptor heterojunctions. Science, **1995**, 270, 1789.

[5] Frederic C. Krebs. Polymeric Solar Cells: Materials, Design, Manufacture. DEStech Publications, Inc., Lancaster, Pennsylvania, **2010.**

[6] Lewis Gomez De Arco, Yi Zhang, Cody W. Schlenker, Koungmin Ryu, Mark E. Thompson, and Chongwu Zhou. Continuous, highly exible, and transparent graphene films by chemical vapor deposition for organic photovoltaics. *ACS Nano*, **2010**, 4(5), 2865.

[7] Vipul Singh, Anil K. Thakur, Shyam S. Pandey, Wataru Takashima, and Keiichi Kaneto. A comparative study of al and lif:al interfaces with poly (3 -hexylthiophene) using bias dependent photoluminescence technique. Organic Electronics, **2007,** 9(5), 790.

[8] M. Girtan and M. Rusu, Role of ito and pedot: pss in stability/degradation of polymer: fullerene bulk heterojunctions solar cells. *Solar Energy Materials and Solar Cells*, **2010**, 94(3), 446.

[9] Jiao Li, Juncheng Liu, Congjie Gao, Jinling Zhang, and Hanbin Sun. Influence of mwcnts doping on the structure and properties of PEDOT:PSS films. *International Journal of Photo energy*, **2009,** article ID-650509.

[10] Frederik C. Krebs. Polymeric Solar Cells: Materials, Design, Manufacture. DEStech Publications, Inc., Lancaster, Pennsylvania, **2010.**

[11] S. Sista, M.-Hyae Park, Ziruo Hong, Yue Wu, Jianhui Hou, Wei Lek Kwan, Gang Li, and Y. Yang, Highly Efficient Tandem Polymer Photovoltaic Cells, *Adv. Mater*., **2010**, 22, 380.

[12] Hao Chen, Linfeng Hu, Xiaosheng Fang, Limin Wu, General Fabrication of Monolayer SnO2 Nanonets for High-Performance Ultraviolet Photo detectors, *Adv. Funct. Mater*, **2012**, 22, 1229.

[13] Kiran Kumar Manga, Junzhong Wang, Ming Lin, Jie Zhang, Milos Nesladek, Venkatram Nalla, Wei Ji, Kian Ping Loh, High-Performance Broadband Photodetector Using Solution-Processible PbSe–TiO2–Graphene Hybrids, *Adv. Mater*., **2012**, 24, 1697.

[14] J. You, Chun -Chao Chen, L. Dou, S. Murase, Hsin-Sheng Duan, S.A. Hawks, T. Xu, H.J. Son, L. Yu, G. Li, Y. Yang, Metal Oxide Nanoparticles as an Electron-Transport Layer in High-Performance and Stable Inverted Polymer Solar Cells, *Adv. Mater*., **2012,** 24, 5267.

[15] National Instruments. Part II - photovoltaic cell i-v characterization theory and labview analysis code, **2012.**

CHAPTER 3

MATERIALS USED AND EXPERIMENTAL TECHNIQUES

3.1 Cell Structure of the investigated device:

Along with the geometry, the different layers used in the devices investigated in this thesis are discussed in this section.

3.1.1 Geometry:-

The organic solar cells investigated in this thesis are based on both conventional as well as inverted structure. The conventional cells have the structure ITO/PEDOT: PSS/P3HT: PCBM/Al, ITO|MoO3|P3HT:PCBM|Al. The inverted cell has the structure ITO|ZnO|P3HT:PCBM| MoO3| Al, ITO|ZnO+PDADMAC|P3HT:PCBM| MoO3|Al, ITO|PFN|P3HT:PCBM| MoO3| Al, ITO|PFN+GRAPHENE|P3HT:PCBM| MoO3| Al. In cells based on normal geometry the transparent ITO electrode behaves as the anode (hole collector) and the back Al electrode serves as the cathode (electron collector). In cells based on inverted geometry, ITO serves as the cathode whereas Al serves as the anode.

3.1.2 The Active Layer:-

For our investigation, we have used donor and acceptor combinations mentioned in literature viz; P3HT: PC60BM whose chemical structures are shown in Figure 3.1. All these chemicals were commercially bought from Sigma-Aldrich, USA. In this thesis, the role of P3HT as the donor polymer has been investigated. P3HT is a widely used semiconducting polymer in polymer solar cells.P3HT is based on thiophene units joined at the 2 and 5 positions in a head -to-tail geometry (Figure 3.1(a)). To be able to dissolve the thiophene a hexyl site group is added in the third position.

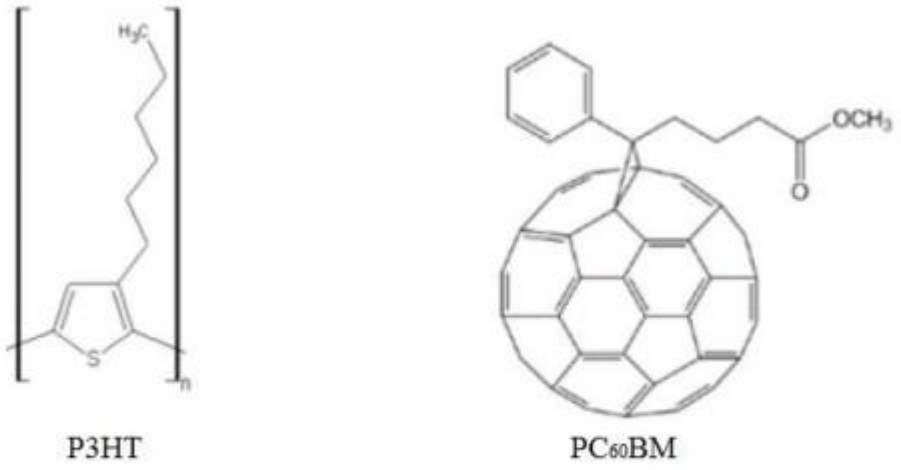

Figure 3.1 Chemical structure of (a) donor polymer P3HT (b) acceptor $PC_{60}BM$

P3HT is semi crystalline in solid state. It has a maxi mum absorption around 500 nm [1]. Due to its electron rich nature and high-energy HOMO level it's a good hole conductor [1]. For a good acceptor, organic materials with high electron affinity are required. Such materials are rare and thus making the choice of acceptors limited [1].The material investigated in this thesis as acceptor is phenyl [6, 6] - C61-butyric acid methyl ester (PCBM) - a soluble C60 based compound (Fig 3.1(b)). PCBM forms crystalline domains in the bulk heterojunction with P3HT and it increases the hole mobility of the polymer.

3.1.3 Electrode Materials:-The following are the requirements for a good electrode (cathode and anode):

- A large difference in the work function of the electrode materials can give rise to a large VOC.
- The front electrode needs to be transparent in order to allow maximum light to enter the active layer and cause photo generation of charge carriers.
- The back electrode is usually a metallic and opaque material.

In view of these requirements we chose Indium Tin Oxide (ITO) as the front electrode and Al as the metallic back electrode. Umicore, a company that specializes in thin film products specifies that the front electrode which is ITO electrode has typical composition ratios of In2O3/SnO2- 95/5, 90/10 and 83/17 wt.% with a band gap of 3.7eV.Here, sheet of resistivity- 4 to 8 $\Omega \cdot sq^{-1}$ is used. The current densities vary from 5-10 mA/cm^{-2}. Further, the work function of ITO depends upon the inter layer above the ITO such as- PEDOT: PSS and ZnO.

3.1.4 Buffer Layers (or interlayers):-

In view of improving the charge transport at the interface between the electrode and the active layer we use buffer layers. This layer facilitates the following functions:

- It protects the organic layer from diffusion of the electrode material into it.
- It prevents the penetration of oxygen and water molecules.

We have chosen PEDOT: PSS, MoO3, ZnO, PFN and ZnO with polymer namely-PDADMAC as the buffer layers for our devices. Poly[(9,9-dioctyl-2,7-fluorene)- alt -(9,9-bis(3 ′-(N,N dimethylamino)propyl)-2,7-fluorene)] (PFN),

Poly-(ethylenedioxythiophene):polystyrensulphonic acid (PEDOT:PSS), which is a hole transporting layer is inserted between the ITO and the active layer. The chemical structure of PEDOT: PSS is shown in Figure 3.2. Along with making the surface uniform, it also enhances the adhesion of the organic active layer onto the ITO (anode).

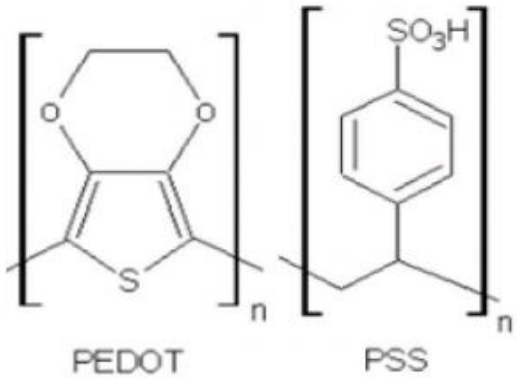

Figure 3.2 Chemical structure of the donor polymer PEDOT and the acceptor PSS

The PEDOT: PSS film is semi-transparent with light blue colour. In terms of conductivity, this layer is able to attain values comparable to that of metals [2]. Along with certain advantages, there are a couple of disadvantages too- due to the hygroscopic nature of PEDOT: PSS, water is introduced in the cell which later causes degradation in organic solar cell. PEDOT: PSS is used as a hole transport layer (HTL). Its work function is around 5.1 eV which is 0.4 eV higher than that of ITO (4.7 eV). This thus leads to a reduction in the injection barrier between the ITO and the active layer. Before coating PEDOT: PSS, UV -ozone treatment of the ITO substrates is usually carried out. This is done to make the ITO surface hydrophilic and to reduce the contact angle with water (discussed in section 4.5). PEDOT: PSS is widely used due to its several advantages such as- high work function (~5.2eV), good conductivity and highly stable oxidized state [3-8].

3.1.5 Polymers:

Poly(diallyldimythylammonium chloride) or PDADMAC

Poly(diallyldimythylammonium chloride) (PDADMAC) is a polymer of diallyldimethylammonium chloride (DADMAC) .The chemical structure is shown in Figure 3.4. It is a high charge density cationic polymer and thus making it suitable for flocculation. It too is soluble in water.

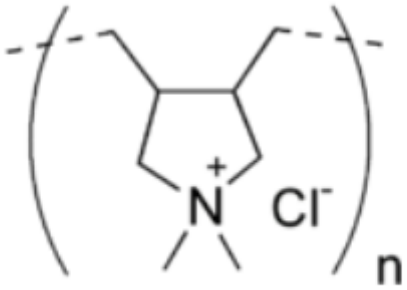

Figure 3.4 Structure of Poly (diallyldimythylammonium chloride) (PDADMAC)

3.2 Experimental Techniques Used:

3.2.1 Standard Glove Box

Due to hygroscopic nature of materials used for organic solar cell fabrication we need to use a glove box with high purity inert atmosphere (such as nitrogen or argon) .Figure 3.5 shows the MBrawn standard glove box used in NPL, New Delhi. The gloves are placed in such a way that the user can place both arms inside and carry out the necessary task inside the glove box. Glove boxes are also used in cases where hazardous materials need to be dealt with. The samples need to be loaded into the ante chamber first. The working inside the glove box is briefly explained:

Loading materials into the antechamber

- Before loading the materials the antechamber needs to be purged.
- Open the gate of the antechamber and load the materials.
- Once loading is complete, the antechamber needs to be evacuated and purged at least thrice so that all of the oxygen and other non-inert gases are removed from the antechamber.

Transferring the materials from the antechamber into the glove box

Insert both arms into the glove box and use the left side of the foot pedal to decrease the pressure inside the box.

- Once the antechamber has been purged at least thrice, open the gates of the chamber and make the necessary transfers.
- It is important to check whether any debris is left behind as this could prevent the gates of the antechamber from shutting properly.
- Now close the gates of the antechamber and evacuate it when working inside the box.

Figure 3.5 Automated Glove Box System with Metallization compartment and Spin coating compartment (NPL, New Delhi)

3.2.2 Spin Coating Technique:

The technique of spin coating is one of the most widely used techniques used for coating in organic solar cells. The ease of reproducing homogenous films using this technique is the prime factor. In this technique, the angular velocity of the substrate causes the excess of the solution over the substrate to be ejected. Centripetal acceleration will cause most of the excess fluid to spread up to the edge of the substrate. In the end a thin homogenous layer is obtained over the substrate. Excess of the solution (or ink) is dropped using a dropper onto the centre of the substrate (Figure 3.6 (a)).Then the substrate is made to rotate at the desired rotation speed i.e. Rpm (rotations per minute) for a particular time interval. It is possible to reproduce the film thickness, morphology and surface topography if the rotation speed (rpm) and time interval are kept constant.

The key stages in spin coating are - deposition, spin-up, spin -off and evaporation [9]. This is depicted in Figure 3.6(b).

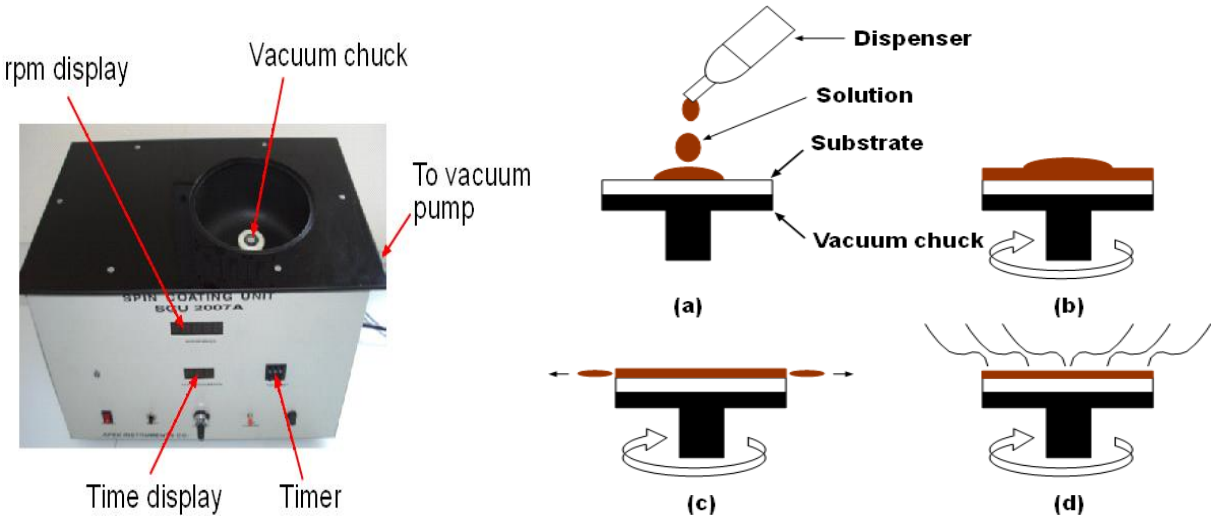

Figure 3.6: Spin Coating Unit and process of spin coating

The spin coating technique is simple enough for laboratory use but is not efficient enough for industrial use. When it comes to commercialization of organic photovoltaic technology where mass scale production is required, it becomes uncompetitive.

3.2.3 Vacuum Technology

In thermal evaporation (discussed in the next section), vacuum technology plays an essential part. Here the different pump technology used will be discussed, namely -rotary pump and turbo pump.

a) Rotary Vane Pump:

The rotary pump is an oil sealed rotary displacement pump. See Figure 3.7. It essentially consists of- a housing (1), an eccentrically installed rotor (2), vanes (3) installed using a spring for radial movement of the rotor, an inlet and outlet (4).

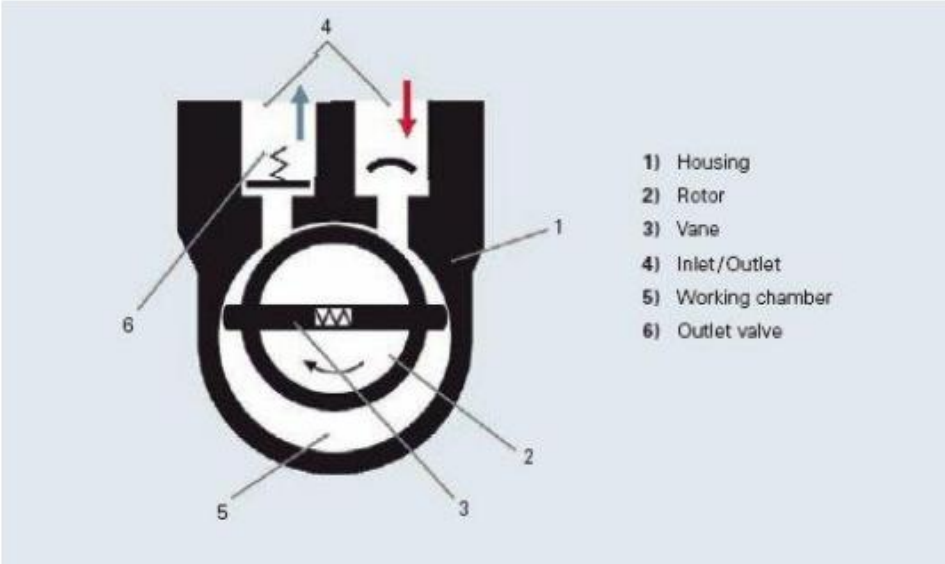

Figure 3.7 A rotary vane pump [10]

The vanes along with the rotor together divide the working chamber into two different spaces with variable volumes. The centres of the rotor and housing are offset thus causing eccentricity. The movement of the rotor leads to two separate variable sized volumes within the working chamber. This in fact gives rise to the pumping action in the motor. The inlet is attached to the space with increasing volume and the outlet is attached to the space with decreasing volume. As the volume of the space increases, a low pressure is generated within the space causing air to flow in from the inlet. Whereas, when the volume in the second space within the working chamber decreases, a high pressure is generated within thus causing the air to be expelled from the outlet connected.

b) Turbomolecular Pump:

Turbomolecular pumps come under the category of kinetic pumps. They are used in ultra-high vacuum (UHV) systems. The mechanism used in this pump is based on the fact that molecules can be given momentum in a particular direction by repeated collision with a solid surface. A rapidly spinning rotor (similar to a turbine rotor) repeatedly hits the gas molecules from the inlet and towards the exhaust. Figure 3.8 shows the lateral view of the inside of a turbomolecular pump. This pump consists of stack of rotor disks. In between rotor disks are stators. As the name suggest stators are stationary disks that contain similar blades as the rotors but oriented in the opposite direction.

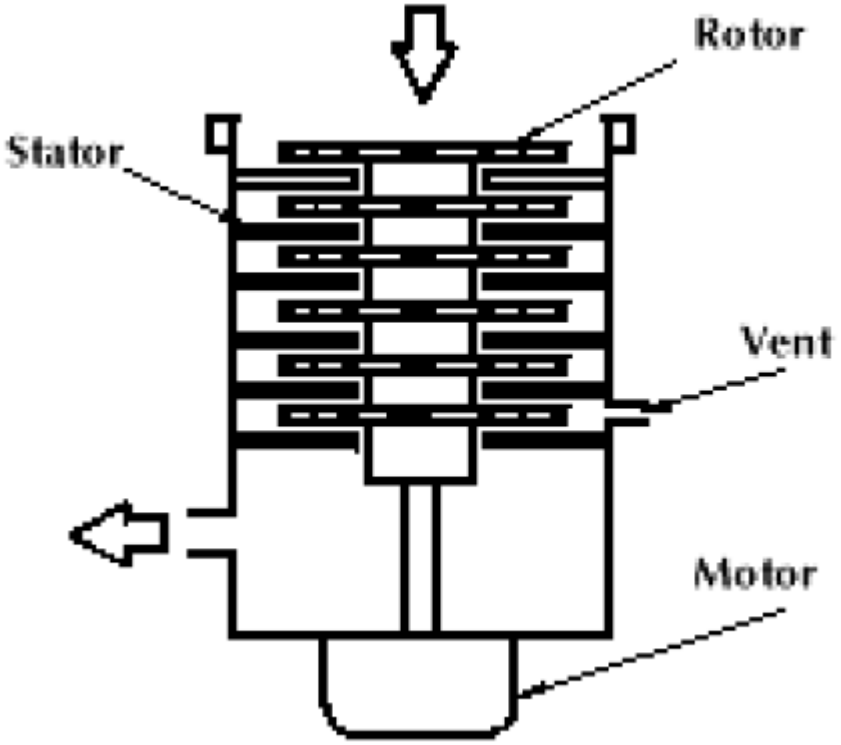

Figure 3.8 Lateral view of turbomolecular pump [11]

3.2.4 Thermal Evaporation Technique:

This technique of deposition incorporates ultra-high vacuum. The material to be deposited is kept on a boat. Here, electric resistance is used to heat the boat to extremely high temperatures. This causes the material kept on the boat to slowly melt and then evaporate onto the substrates kept above for deposition. The presence of ultra-high vacuum assures the formation of impurity free film on the substrate as impurities of the residual gas present in the working chamber is absent. Also in vacuum the vapour reaches the substrate without any collisions or scattering with other gas phase atoms in the chamber (Figure 3.9).

Thermal evaporation is one of the simplest processes of depositing material onto a substrate. One major drawback is the wastage of the material during deposition.

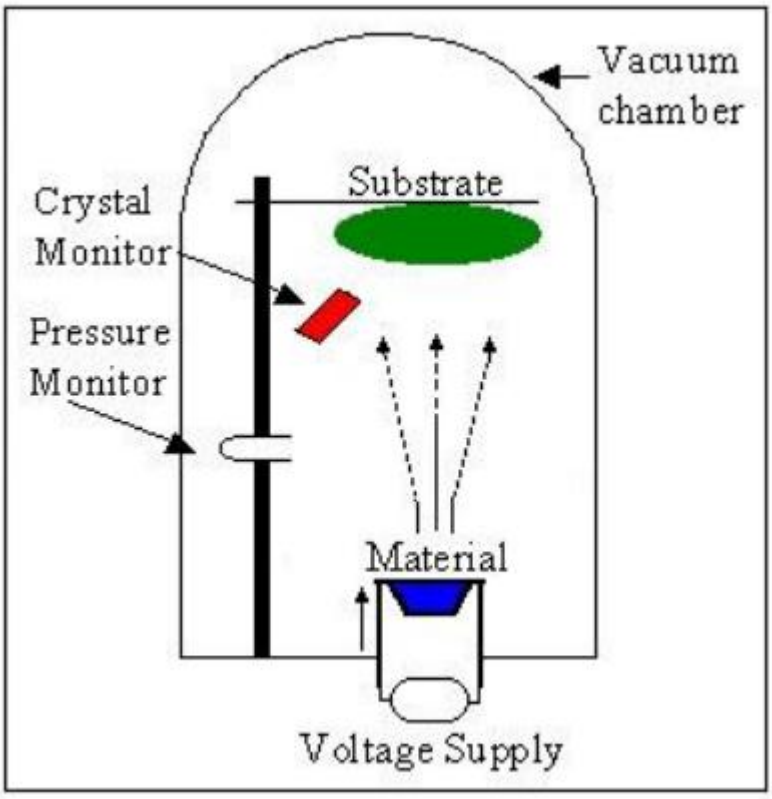

Figure 3.9 Thermal evaporation process

The specifications of the system are mentioned below .

Specifications:-

- Chamber pressure ~ 1 x 10^{-5} to 5 x 10^{-5}mbar.
- Typical filament current varies from 10 to 200 Amps.
- Tungsten or Molybdenum boats used to heat the evaporants.
- Maximum deposition thickness ~ 600 nm.

3.3 SEM principle:

The scanning electron microscope (SEM) is a powerful and frequently used instrument, in both academia and industry, to study, for example, surface topography, composition, crystallography and properties on a local scale. The SEM has an extremely large depth of focus and is therefore well suited for topographic imaging. Besides surface topographic studies the SEM can also be

used for determining the chemical composition of a material, its fluorescent properties, the formation of magnetic domains and so on.

The specimen is bombarded by a convergent electron beam, which is scanned across the surface. This electron beam generates a number of different types of signals, which are emitted from the area of the specimen where the electron beam is impinging, as shown in figure.

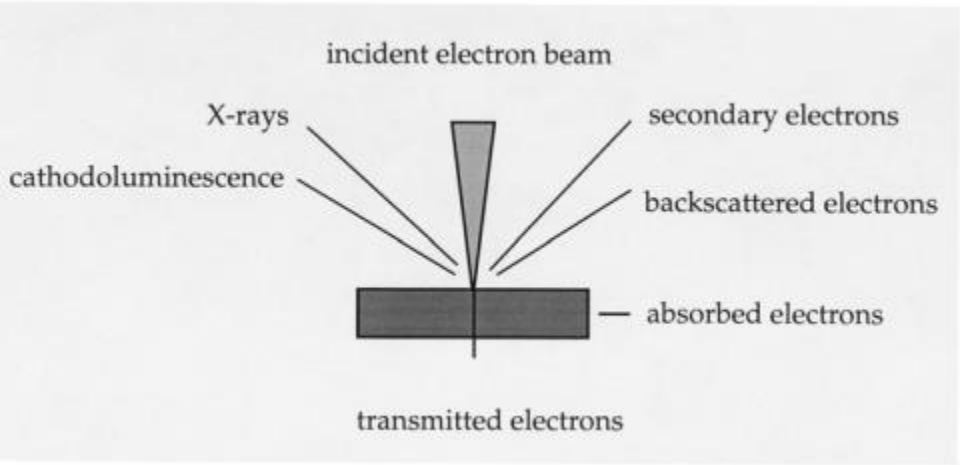

Figure 3.10 Some of the different types of signals produced when high-energy electron impinge on a material.

The induced signals are detected and the intensity of one of the signals (at a time) is amplified and used to as the intensity of a pixel on the image on the computer screen. The electron beam then moves to next position on the sample and the detected intensity gives the intensity in the second pixel and so on. The working principle of the SEM is shown in Figure 3.11.

The SEM can be operated in many different modes where each mode is based on a specific type or signal like Secondary electrons (SE), Backscattered electrons (BE), Electron backscattered diffraction (EBSD), X-ray ,Absorbed current, Transmitted electrons etc. The choice of operating mode depends on the properties of the sample and on what features one wants to investigate. Surface topography can be observed either in the SE mode or in the BE mode.

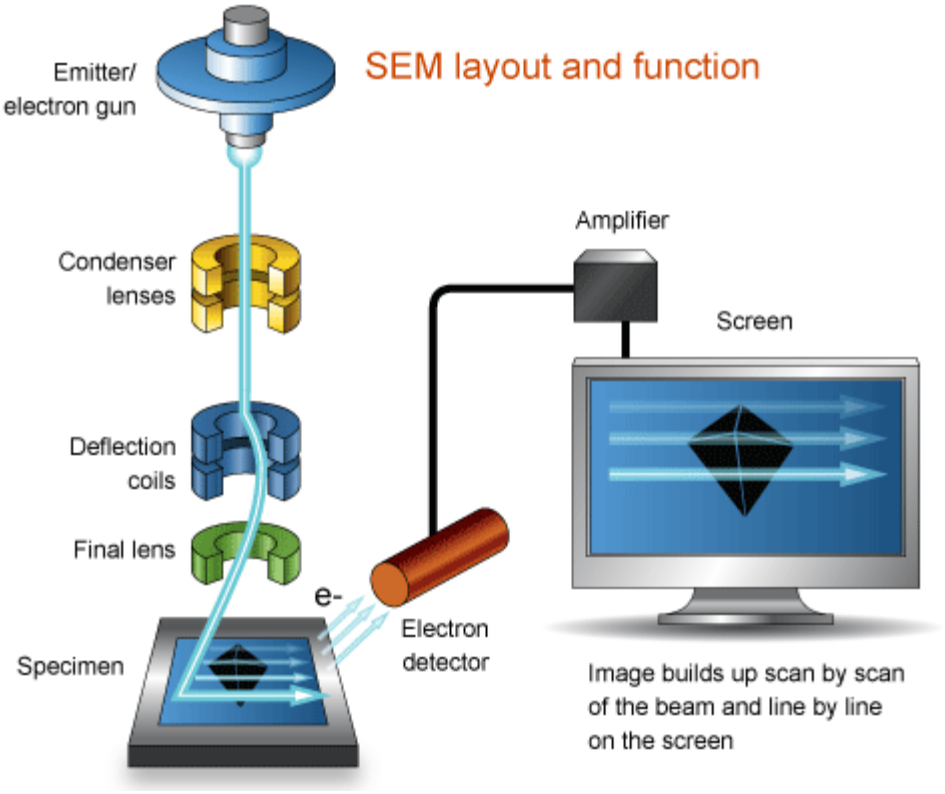

Figure 3.11 SEM layout and function [12]

3.4 Photoluminescence(PL) Principle: Photoluminescence is the process in which an atom absorbs a photon causing transition to higher electronic energy state and releases photon while relaxing back to its ground state. The resulting photon has the energy difference between the two electronic energy states involved in transition.

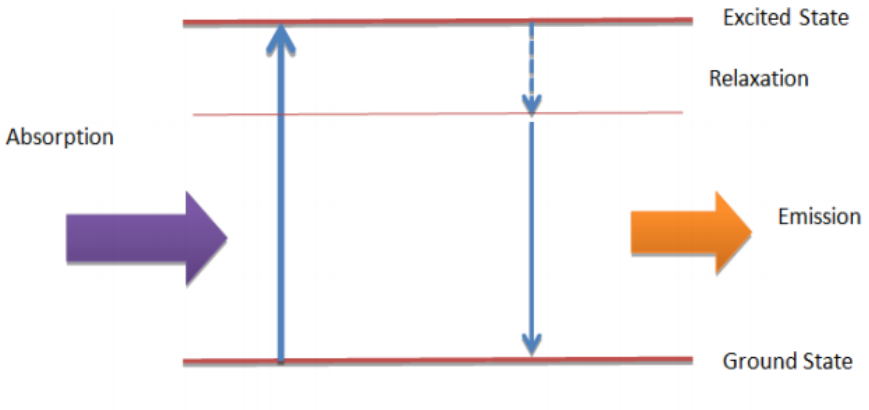

Figure 3.12 Photoluminescence process in an atom- absorption, excitation, non-radiative relaxation and emission [13]

Experimental setup:

Photoluminescence is a versatile, contactless, nondestructive method of investigating the electronic structure of the material. The setup of photoluminescence spectroscopy is given in Figure 6.21. It consists of a Laser source, a spectrophotometer and a detector. The laser beam is focused on the sample with the help on focalization lens. The emitted light is collected by either one lens or two lenses with focal lengths F1 and F2. The two lenses are used to make use of smaller focal length F1 to increase collection efficiency of emitted light. Also F2 is used to match the optical aperture of spectrometer avoiding any further loss of emitted light [13,14].

PL spectroscopy gives information on low lying energy levels of the valence band. During the experiment the excitation provided by laser is much larger than the band gap of the material. The photoexcited charge carriers- electrons and holes relax in their respective bands and recombine to give emission of photon. The samples were prepared in chlorobenzene as solvent and the measurements were carried out at room temperature. The PL signal was detected with Perkin Elmer LF55 having Xenon spectrophotometer.

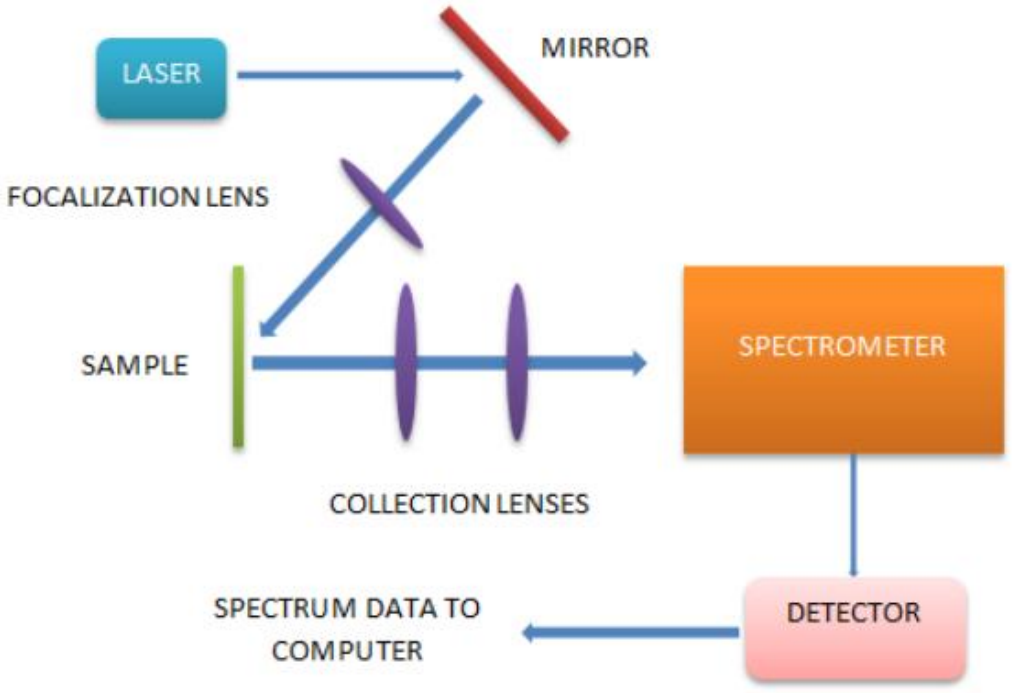

Figure 3.13 Basic schematic diagram of a typical photoluminescence experimental setup.

3.5 Profilometry Principle:

STYLUS Profilometry is one of the common tools to measure surface film characteristics. In the study of the surface mechanical properties of any material, the topography can be of significant importance in understanding the behavior of the material. Therefore it is a crucial step to be able to accurately characterize the topography of the surface prior to mechanical analysis, as well as the deformation, degradation and changes induced by the analysis.

The concept behind confocal profilometry involves the use of the chromatic aberration (CA) principle. By directing a white light source through a filtering optical component towards a sample surface it is possible to use the chromatic aberration to separate the light with a dispersive lens into its component wavelengths, each of which corresponds to a different z-coordinate in the optical axis. Therefore the visible light spectrum is now encoded with z-coordinate data as a function of varying focal distance from the end of the lens.

As the focus point of each wavelength is represented at a different distance from the lens, the returning light waves will be different according to the height characteristics of a specific region of the sample. Therefore the returning spectrum at any given point can be regarded as the spectrophotometric signature of z-height, where strong spectral response is indicative of a defined distance away from the lens at a given focal point.

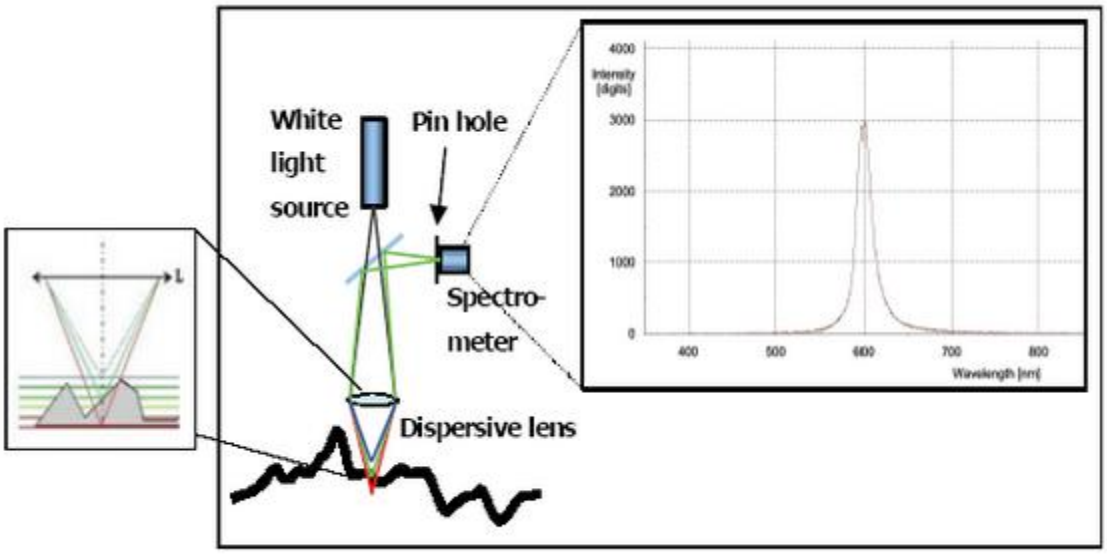

Figure 3.14 Profilometry layout and function [15]

For example I analyze the thickness of buffer layer ZNO-PDADMAC which is spin coated on glass sheet at different revolution per minute(RPM). The results obtained as follows

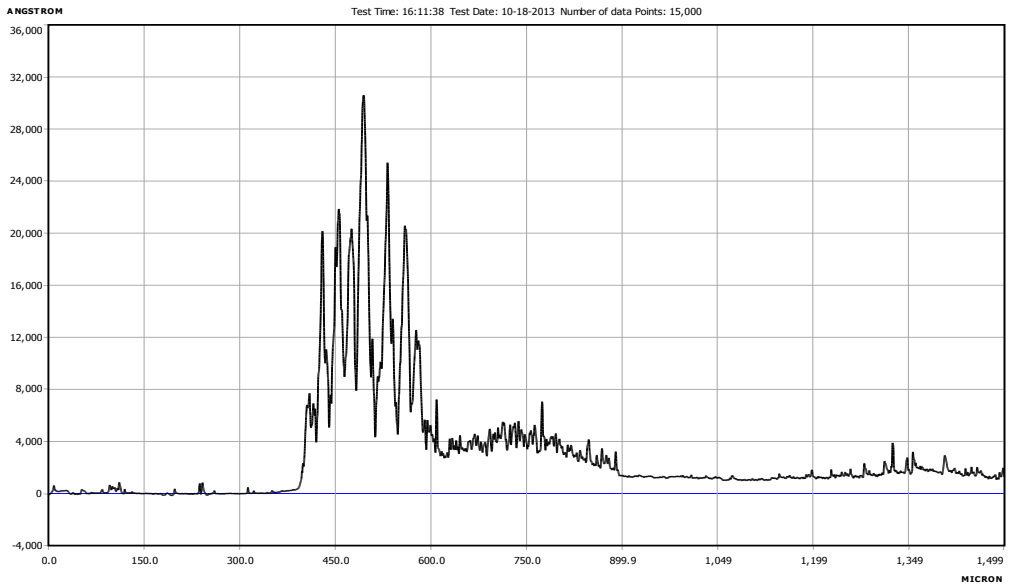

Figure 3.15 Profilometry screen of ZnO-PDAMAC as buffer layer at 3500rpm(NPL,Delhi)

3.6 References:

[1] Jørgensen, M., Bundgaard, E., Bettignies, R.d., and Krebs, F.C., International Society for Optical Engineering, Tech. Univ. of Denmark, **2008**, 11.

[2] R. Schlaf, H. Murata, Z.H. Kafafi, Work function measurements on indium tin oxide Films, *J. Electron Spectrosc. Relat. Phenom*, **2001**, 120, 149.

[3] J. Y. Kim, J. H. Jung, D. E. Lee, and J. Joo, *Synth. Met.*, **2002**, 311, 126.

[4] J. Hwang, F. Amy, and A. Kahn, *Org. Electron.*, **2006**, 7, 387.

[5] H. W. Heuer, R. Wehrmann, and S. Kirchmeyer, *Adv. Funct. Mater.* , **2002**, 12, 89.

[6] W. W. Chiu, J. Travaš-Seidić, R. P. Cooney, and G. A. Bowmaker, *Synth. Met.*, **2005**, 155, 80.

[7] N. Koch, A. Vollmer, and A. Elschner, *Appl. Phys. Lett.*, **2007**, 90, 043512.

[8] Y. J. Lin, H. C. Chang, and B. Y. Liu, *Appl. Phys. Lett.*, **2007**, 90, 112112.

[9] Niranjan Sahu, B Parija and S Panigrahi, Fundamental understanding and modeling of spin coating process: A review, *Indian J. Phys*., **2009**, 83 (4), 493.

[10] Vacuum generation- rotary vane vacuum pumps, Pfeiffer Vacuum, official website.

[11] Kurt J. Lesker and Company. Turbomolecular Pumps and Drag Pumps: Technical Notes.

[12] SEM layout and function http://www.ammrf.org.au/

[13] Mark Fox, "Optical absorption of solids", Oxford University Press Inc., (2001)

[14] Website: http://www.lpa.ens.fr/spip/spip.php?article226&lang=en

[15] Website: http://www.csm-instruments.com/

CHAPTER 4

BHJ SOLAR CELL FABRICATION

4.1 Etching of the ITO glass sheet:

ITO glass sheets were first cut into 2 X 2 inch substrates using a diamond cutter. These substrates were then subsequently etched using a laser scriber. Two vertical stripes each of 0.6 cm were left out and the remaining ITO was etched. These stripes later helped in the formation of a pixel. In the pattern used, four such pixels were present once device fabrication was complete. Each pixel would function as a different and independent solar cell. Now these patterned ITO substrates need to be thoroughly cleaned before device fabrication.

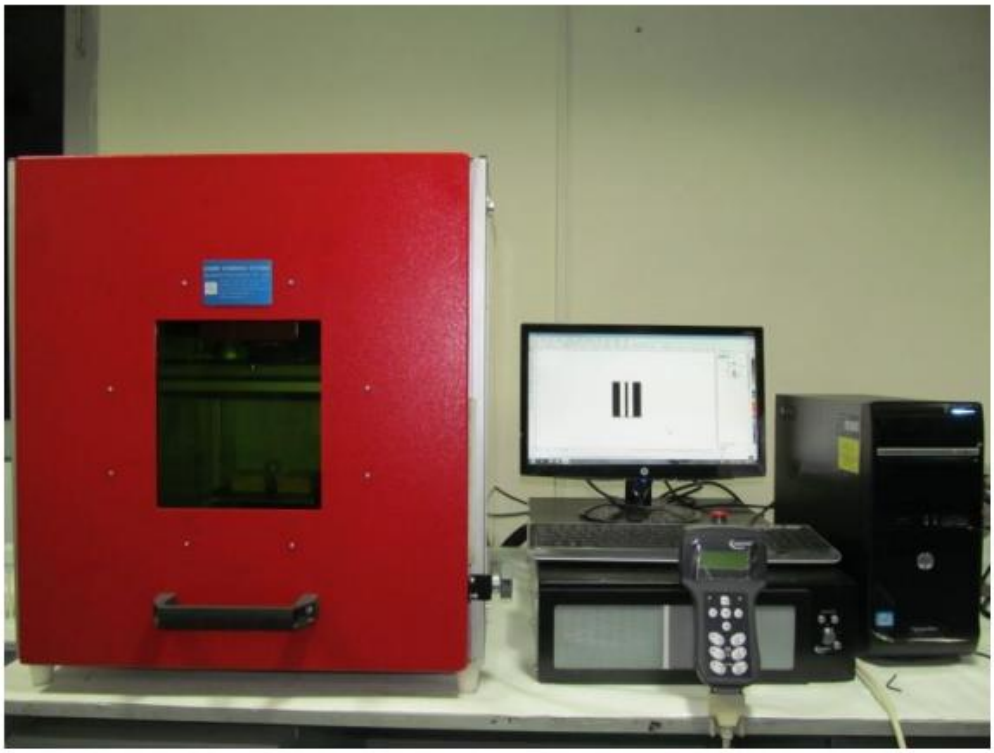

Figure 4.1 Picture of Laser Scribing Unit used in NPL, Delhi

4.2 Preparation of Active Material:

In this thesis two active material (donor polymer: acceptor fullerene combination) have been investigated- P3HT:PC60BM. As previously discussed in section 3.1.2, P3HT is donor polymer whereas fullerene compound PC60BM behave as acceptor. The weight ratios used for the preparation is: P3HT:PC60BM- 3:2 wt. ratio.

The solvent used in both the cases is chlorobenzene (each 1 ml).

Both these active layer combinations are stirred using a magnetic stirrer. The P3HT:PC60BM combination was stirred 24 hours of stirring before use.

4.3 Preparation of Buffer Layer Solutions:

The buffer layers solutions were synthesized using solution route. The following buffer layers were used for the present investigation

For conventional device-:

- PEDOT:PSS
- MoO3 film

For inverted device-

- ZnO film
- ZnO – PDADMAC nanocomposite film
- PFN film

ZnO Solution:

0.10-0.235 g of zinc acetate dihydrate was added in 5 ml propanol and allowed to stir for 5 min. A white cloudy solution is obtained here. Now after 5 minutes, few drops of diethanolamine (DEA) are added to this solution. DEA acts as a stabilizer. Slowly we will observe that the cloudiness disappears and a colourless and transparent solution is obtained. Now, this solution is stirred at 60°C for 2 hours. The solution is then kept untouched and undisturbed for 24 hours. After coating this solution on ITO, the substrate is heated at 200°C for 30 minutes.

ZnO-PDADMAC nanocomposite solution:

To make PDADMAC solution we added 0.5 ml PDADMAC in 0.5 ml of water. This solution was stirred for 30 minutes. Now to prepare the nanocomposite solution, this 1 ml PDADMAC solution was added in 2 ml of ZnO solution. Also after a 5 minute interval, 2 to 3 drops of DEA were added in this solution and the resultant mixture was then stirred for 30 minutes.

PFN solution:

The PFN interlayer material was dissolved in methanol (5 ml) in the presence of a small amount of acetic acid (2 µl ml^{-1}) and its solution (concentration, 2 mg ml^{-1}). This solution was stirred for 24 hours.
All the previously mentioned chemicals were commercially purchased from Sigma Aldrich, USA.

4.4 Cleaning of the ITO glass slide:

First the glass slides were wiped using a tissue dipped in acetone. Here all the dust and other particles are removed from the glass slides (or substrates). Following this, the slides are ultra - sonicated in a beaker filled with soap water. Here further other micro-sized impurities are removed. Ultrasonic cleaning is the process in which sound is used to produce bubbles by agitation of a liquid (mostly water). This agitation produces high forces on impurities and helps in loosening contaminants tightly adhered to the glass surface [1]. This is allowed to continue for another 20 minutes.

Figure 4.2 Ultrasonic cleaning of substrates (in beaker)

Once the ultrasonic cleaning process is complete, the slides are further rubbed with soap using cotton. This process of rubbing with soap is carried out until a proper thin layer of water stays on the glass surface. This step is particularly done to remove any oil contaminants from the glass surface (as shown in Figure 4.3).

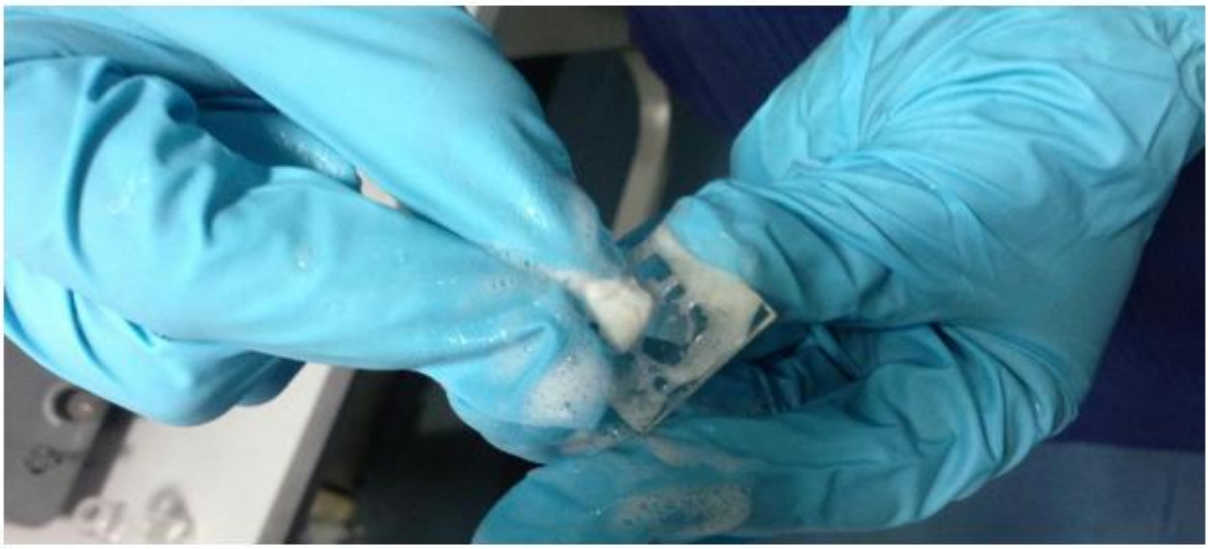

Figure 4.3 Soap Cleaning of ITO substrate

After completion of the above, a three step boiling process is carried out. In the first step the glass substrates are boiled in acetone for 15 to 20 minutes. Boiling is carried out with the help of

a substrate holder. Each holder can hold upto 8 ITO substrates (Figure 4.4). Acetone removes all the tiny water droplets that were stuck to the substrate. In the next step these substrates are boiled in trichloroethene (TCE) for another 20 minutes. While making the transfer, the fumes expelled during boiling, aid in substrate drying. TCE removes acetone completely from the glass surface. Also in this step if any impurities are still left, they can be removed physically using cotton wrapped around a clean tweezer. In the last and final step, the glass substrates are boiled in iso-propanol (ISP) for 15 minutes. Boiling propanol removes the remaining TCE from the substrates.

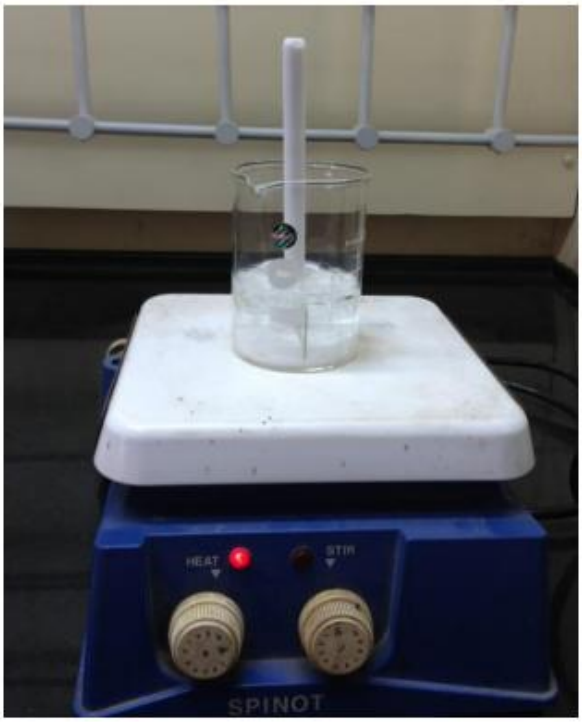

Figure 4.4 Boiling of the ITO substrates

4.5 UV-Ozone Treatment:

This treatement is undergone in the standard glove box used in National Physical Laboratory (NPL), New Delhi. Here we expose the ITO substrates to ozone. ITO is widely used as an electrode material in organic photovoltaics (OPVs).The morphology of the ITO surface and the oxygen defects are known to be important factors in determining the charge injection at the interface [2]. Treatments such as chemical treatment (aquaregia, RCA), and plasma treatment, and UV-ozone treatment have been developed to improve the charge injection from the ITO into

the organic layer [4-6].These treatments can increase the ITO work function, which may be due to surface carbon removal, creation of surface dipoles, a change in the ratio of surface constituents (Sn, In, O). This increase in ITO work function can cause an increase in the hole-injection efficiency from the ITO to the hole -transporting layer [3]. UV-ozone treatment also causes the ITO surface of the substrate to be hydrophilic (i.e. the contact angle for water decreases) and thus assisting in the uniform and homogenous layer formation over the ITO.

Once the ITO glass substrates are kept face up, the working chamber is closed. Now oxygen gas is purged inside the chamber. This purging takes place for 60 seconds after which UV light is radiated inside the chamber. This converts the existing oxygen gas into ozone gas. The duration for this UV radiation is 600 seconds. Next finally nitrogen gas is passed in the chamber. This is done as once the process completes, the inert gas atmosphere is maintained inside the glove box.

4.6 Buffer Layer Coating:

4.6.1 For conventional cells:

Once the UV-ozone treatment of the ITO substrates is completed, the buffer layer coating can begin. The buffer layer used here is a hole transport layer (HTL) as the holes in a conventional structured cell move towards the ITO electrode (anode). The coating technique used here is spin coating. Two HTLs have been investigated, namely-MoO3 and PEDOT: PSS. However, before spin coating the PEDOT: PSS, it needs to be filtered. PTFE hydrophilic filter was used for filteration. This filter is attached to asyringe. This system is then used to filter and then drop the PEDOT: PSS solution onto the substrate for spin coating. The equipment used for spin coating is shown in Figure 4.5. Employing PEDOT: PSS has its pros and cons (as discussed in section 3.1.4).

4.6.2 For inverted cells:

In case of inverted structure, ZnO films have been coated for investigation. Further, ZnO – PDADMAC nanocomposite and PFN films has also been investigated in this thesis. ZnO lowers the work function of the electrode (ITO) and thus the electrons instead of moving towards the metallic electrode, moves towards ITO thus, making ITO the cathode.

Figure 4.5 Picture of Spin Coating System in NPL, New Delhi

4.7 Annealing of Buffer Layer:

4.7.1 PEDOT: PSS (For conventional cells):

Once PEDOT: PSS is coated over the ITO substrate, this buffer layer now has to be annealed at 120°C for 10 minutes. This is done so at to dry the PEDOT: PSS layer as it is water soluble. Thermal annealing of PEDOT: PSS is known to increase the short circuit current density and change the work function of the layer.

4.7.2 ZnO films (For inverted cells):

ZnO film is based on water and thus needs to be heated at 200°C for up to 30 minutes. This causes all the excess water to boil and evaporate, leaving just the film. Care was taken while cooling the substrate. Cooling was done slowly as abrupt cooling can disturb the surface morphology.

4.7.3 PFN films (for inverted cells):

Once PFN is coated over the ITO substrate, PFN film is based on methanol this buffer layer has to be annealed at 100^{o}C for 10min. This can be done to provide uniform surface morphology.

4.8 Active Layer Coating:

In this work, P3HT:PC60BM is the active layer used for conventional devices. This active material is a well-known material and has been dynamically used in organic photovoltaics.

While selecting active materials for use, two important parameters are - the absorption of the active material in sunlight as well as the surface morphology after the coating process is complete. The above two parameters have been studied in detail in the coming chapters. Again the coating method used is spin coating technique similar to PEDOT: PSS. I have selected P3HT:PC60BM for both conventional and inverted devices.

4.9 Active Layer Annealing:

Annealing of the active layer is the key to obtaining optimum values of current and fill factor. Annealing of the active layer (P3HT:PC60BM) was carried out in inert glove box environment (nitrogen environment) at 120°C for 10 minutes. This process should not be carried out in air as oxygen diffuses into the active layer and degrades the material. The changes in surface morphology due to thermal annealing have been noted in the results section. Once annealing is complete next is the thermal evaporation step.

4.10 Thermal Evaporation:

In both conventional as well as inverted cells, aluminium is deposited by thermal evaporation. The only additional step required in case of inverted cells is the deposition of MoO3 just before aluminium and in conventional when MoO3 evaporated used as an interfacing layer thermal evaporator is used. As described in section 3.2.4, this process involves the current heating of a filament (or boat) in a vacuum chamber. Ultra high vacuum (UHV) is needed for this process.

(a)

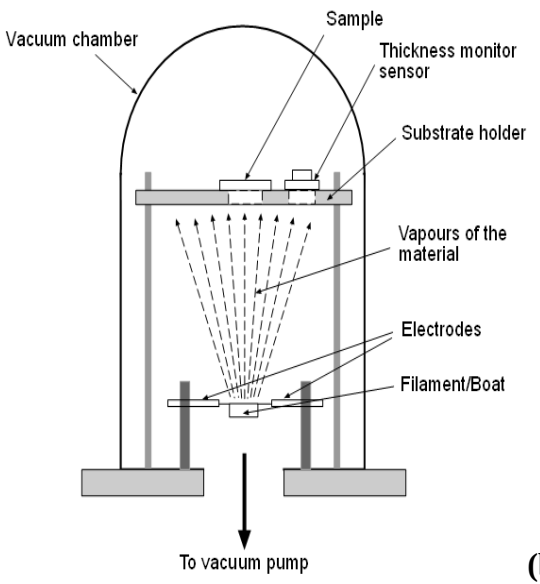

(b)

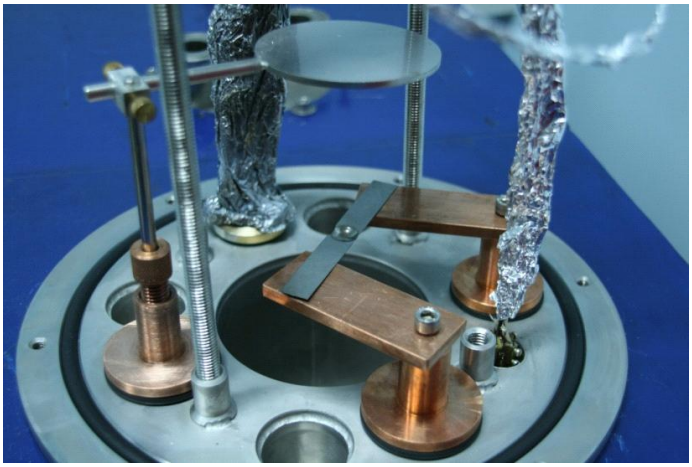

(c)

Figure 4.6 (a) Thermal Evaporation Unit, (b) Working of thermal evaporation system at NPL, New Delhi, and (c) Filament inside the vacuum chamber

Pressure up to 9 x 10^{-6}mbar was attained in the chamber. The process specifications used are:

MoO3 deposition: (For inverted cells and conventional device)

- Power- 30 W
- Deposition Rate- 0.5 A°/sec
- Thickness-7.5-8 nm

Aluminium deposition: (For both -inverted as well as conventional devices)

- Power-35 W
- Deposition Rate- 5 A°/sec
- Thickness-125 nm

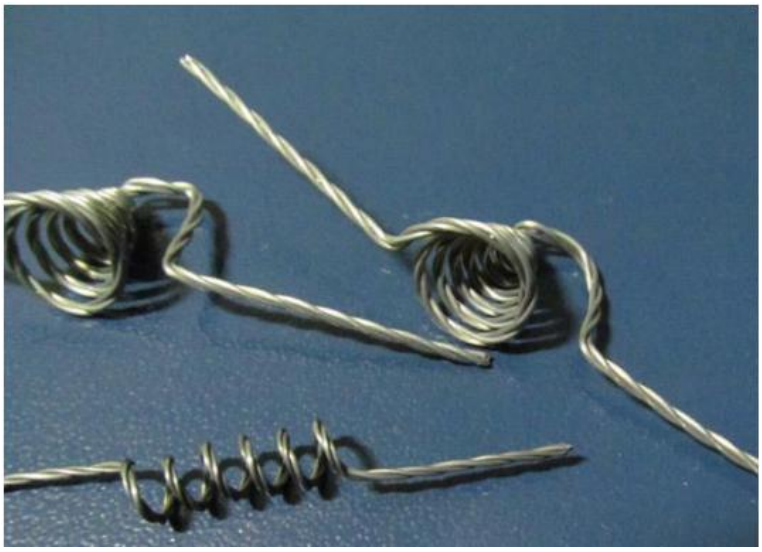

Figure 4.7 Filaments used in thermal deposition process

Once deposition is complete, air is slowly passed into the chamber. The rate is maintained low so as to avoid any major dust particles from entering the chamber and settling on the substrate.

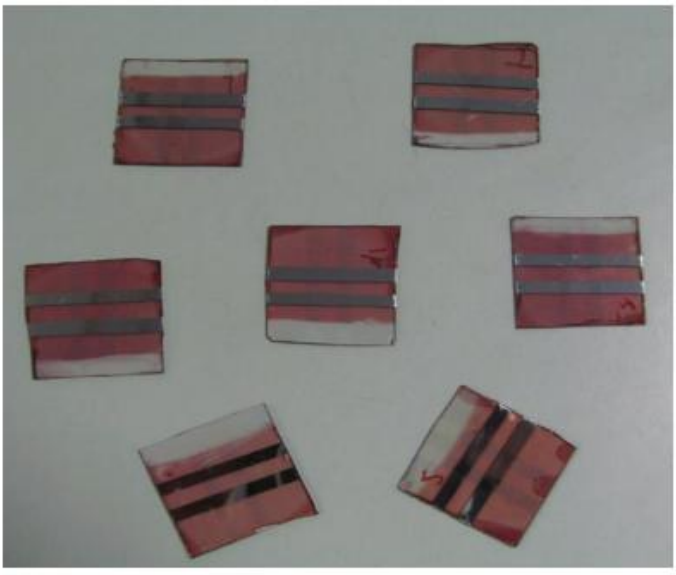

Figure 4.8 Organic Solar Cells Fabricated

4.11 J-V Characterization of the Device:

Once the above steps are complete and the device is fabricated, J-V Characterization of the device is carried out. Here, the cell is illuminated under simulated AM1.5G Illumination at 100 mW/cm^2 (Figure 4.9) using a light source having tungsten halogen lamp from Osram, Germany. The current density characteristics of the device were recorded using Keithley 2420 Source Meter interfaced with a computer. The measurements were done both in illuminated and dark conditions.

Depending on the structure of the device, the positive and negative terminals of the Keithley unit are attached with the anode and cathode terminals of the device respectively. Using the current and voltage characteristics fill factor (FF), open circuit voltage (VOC), and power conversion efficiency (η) were measured.

Figure 4.9 Set-up for J-V characterization of the device.

This entire fabrication process is depicted in Figure 4.10.

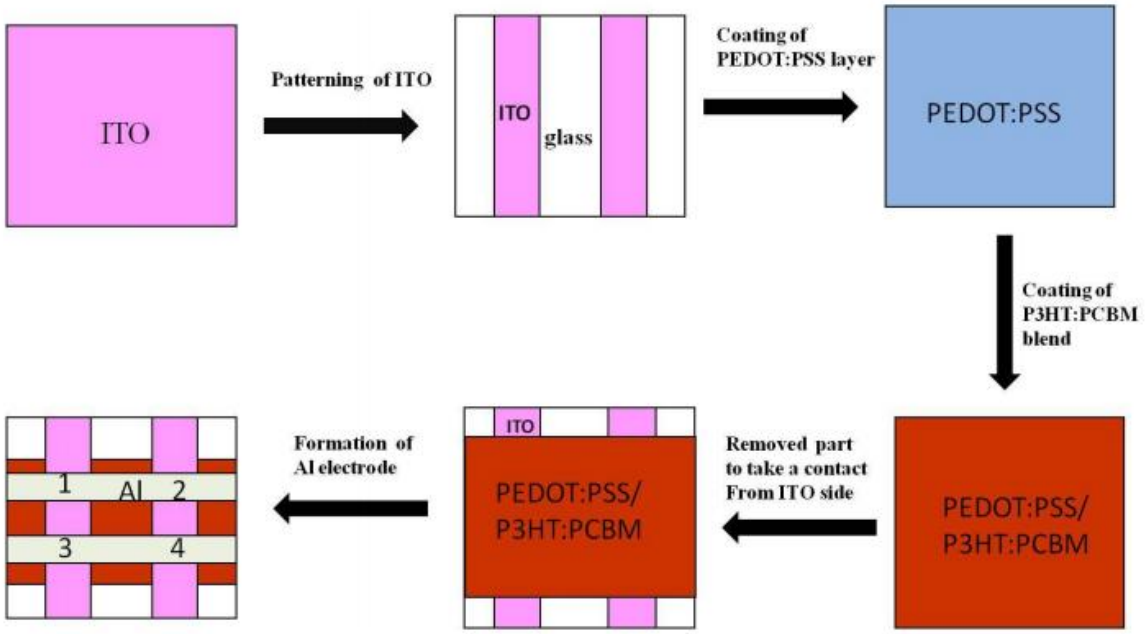

Figure 4.10 Schematic diagram of complete process for fabrication of a typical BHJ solar cell using PEDOT: PSS as the anode buffer layer and P3HT:PC60BM as the active layer.

4.12 References:

[1] Ensminger Dale, Ultrasonics: data, equations, and their practical uses, CRC Press (Taylor & Francis Group), **2009**, 10. 328.

[2] H. K. Lee, J. H. Seo, Y. K. Kim, J. H. Kim, J. R. Koo, K. H. Lee and S. S. Yoon, *J. Korean Phys. Soc.*, **2006**, 49, 1052.

[3] Niranjan Sahu, B Parija and S Panigrahi, Fundamental understanding and modeling of spin coating process: A review, *Indian J. Phys.,* **2009,** 83 (4), 493.

[4] E. Aminaka, T. Tsutsui and S. Saito, *J. Appl. Phys*., **1996,** 79, 8808

[5] S. A. Van Slyke, C. H. Chen, C. W. Tang, *Appl. Phys. Lett*., **1996,** 69, 2160

[6] J. S. Kim, F. Cacialli, A. Cola, G. Gigli and R. Cingolan, *Appl. Phys. Lett***., 1999**, 75, 19

CHAPTER 5

STUDY OF DEVICE PARAMETERS

5.1 Introduction

To estimate solar cell performance and thus further to simulate, design, fabricate, and quality control solar cells, an accurate knowledge of their parameters from experimental data is of vital importance. The electrical characteristic of a solar cell can be described by the equivalent circuit of the single-diode model, the two-diode model[1], or the three-diode model[2-3].

Among these circuit models, the single-diode model has the simplest form as shown in Fig.1. Although the single-diode mode is simple, it can well describe the characteristics of various solar cells, satisfy most of the applications, and thus becomes the most widely used circuit model. In the single-diode model, the relation of the current and the voltage is given as

$$I = I_0\left(\exp\left(\frac{q(V - R_sI)}{nk_BT}\right) - 1\right) + \frac{V - R_sI}{R_{sh}} - I_{ph}, \qquad (1)$$

Where I_0 is the saturation current, I_{ph} the photocurrent, R_s the series resistance, R_{sh} the shunt resistance, n the ideality factor, q the electron charge, k_b the Boltzmann constant, and T the temperature.

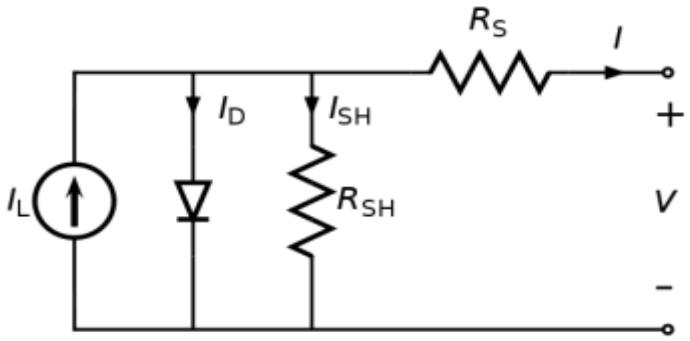

Figure 5.1: An equivalent circuit of a solar cell; adapted from [4]

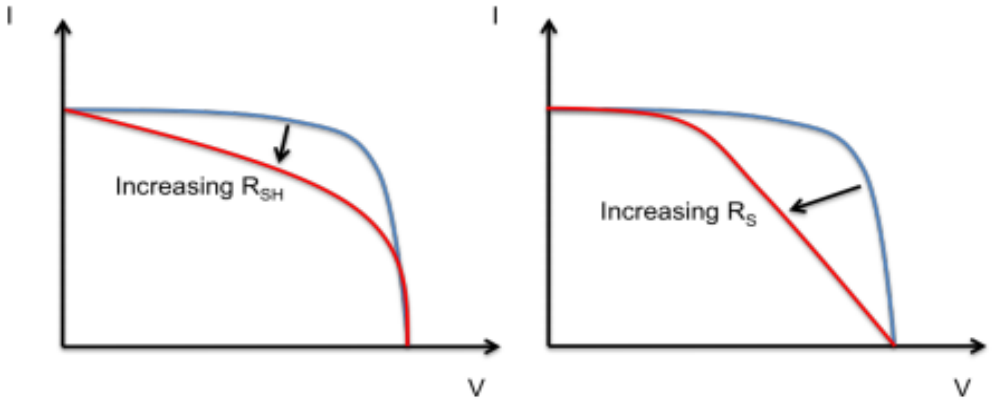

Figure 5.2: The effect of R_{sh} and R_s on a solar cell's IV curve; adapted from [4]

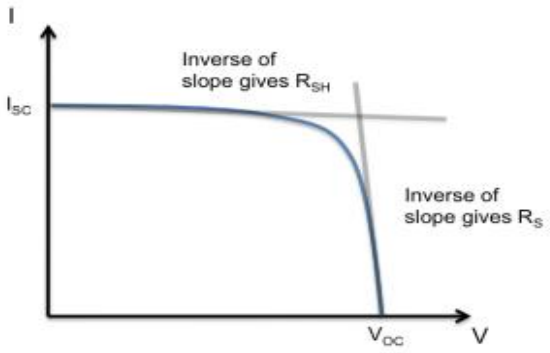

Figure 5.3: Determine R_s and R_{sh} using IV curves; adopted from [4]

According to equation (1), the J–V curve of the solar cell is generally divided into three regions both in the dark and under illumination (Fig. 4) [5]. Actually, if the photocurrent doesn't vary with the applied voltage, the J–V curve under illumination can be seen as the translational dark J–V curve (moved down by J_{ph}) From Fig. 4, it can be seen at negative voltages and low positive voltages (Region I), the J–V curve is a straight line with a slope determined by the 1/Rsh; at intermediate positive voltages (Region II), the J–V curve is an exponential line (J depends exponentially on V), the characteristic of which is determined by the diode; and at high positive voltages (region III), the J–V curve is a second straight line with the slope controlled by 1/Rs. It can be seen apparently that in Region III, if Rs becomes larger, the rise of J with increasing V will get slower (1/Rs=dJ/dV), then the slope of the J–V curve will decrease correspondingly, leading to less ''squareness'' of J–V curve, and a lower FF. Similarly, in Region I, if Rsh decreases, the slope of the J–V curve will increase. Then the J–V curve around J_{SC} becomes less parallel to the x-axis, which will reduce the ''squareness'' of J–V curve and FF, too, while in region II, the J–V characteristic is determined by the diode.

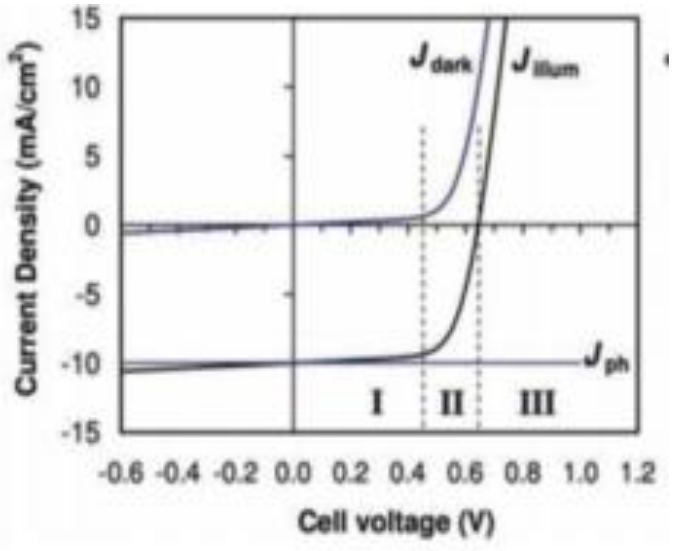

Figure 5.4: Typical J–V plot for an organic solar cell under dark and illumination. The three regions indicated account for where different effects dominate: Region I accounts for leakage (shunt) currents, Region II recombination currents, and Region III series resistance.

The equivalent circuit for a generic solar cell is shown in Figure 5.1, and is noted to have the following current-voltage relationship:

$$I_{total} = I = -I_{photocurrent} + I_{diode} + I_{shunt} \quad \textbf{(2)}$$

$$I = -I_{ph} + I_0\left(\exp\left[\frac{V+IR_s}{nV_{th}}\right] - 1\right) + G_{sh}(V + IR_s) \quad \textbf{(3)}$$

where I_0 is the reverse saturation current, n is the diode ideality factor, $V_{th}=k_BT/q$ is the thermal voltage, R_s is the series resistance and G_{sh} is the shunt conductance ($G_{sh}=1/R_{sh}$).

The most frequently reported solar cell parameters are the open-circuit voltage, short circuit current, fill factor and power conversion efficiency. These values are described in Introduction chapter and are straightforward to calculate from solar cell output characteristics. However, the shunt and series resistances, which are arguably the next most useful parameters for organic solar cells, are not as simple to ascertain. In recent studies on organic solar cells, researchers used the slope of the output curve under dark conditions at V=0V and V=2V to find the shunt and series resistances respectively [6]. This very simple approach was described many years earlier for CdS thin film solar cells [7], and involves the assumption that the series resistance is small and the shunt resistance is large. This approach generally provides reasonable values for the shunt resistance based on the logic shown below:

R_{shunt}: $I_{ph} \approx 0$ (dark output), so

$$I = I_0\left(\exp\left[\frac{V+IR_s}{nV_{th}}\right] - 1\right) + G_{sh}(V + IR_s)$$

At the current axis V=0V, I is small and if R_s is small,

$$\exp\left[\frac{V+IR_s}{nV_{th}}\right] \cong \exp[0] = 1$$

Further, G_{sh} is generally small because R_{sh} is ideally large, so $G_{sh}IR_s$ must be very small.

We can therefore write, by means of simple logic:

$$I \cong I_0(1-1) + G_{sh}V + G_{sh}IR_s \cong G_{sh}V$$

$$I \cong G_{sh}V \; or \frac{dI}{dV} \cong G_{sh} \quad \therefore \frac{dV}{dI}(V = 0V) \cong R_{sh}$$

However, as noted above, this method is only valid under the condition that the solar cell has reasonably good properties with a high R_{sh} and low R_s. Furthermore, the calculation for R_s is only valid if a 'good' voltage point is chosen for the slope calculation. In the study of organic solar cells, especially with new materials and varying solar cell architectures, the assumptions of low R_s and high R_{sh} are not strictly valid. In order to obtain more accurate values for both the series and shunt resistances as well as the diode parameters of the solar cell, one must fit the solar cell parameters to the current equation shown in (1) above.

5.2 Factors that influence performance of OSCs:

5.2.1 Series resistance(R_s):

R_s is one of the important factors that limit the FF of solar cells [8-10]. Generally Rs consists of (1) bulk resistance of the active layer and kinds of functional layers in the film, (2) bulk resistance of the electrodes, (3) contact resistance of every interface in the device and (4) probe resistance. In the fabrication of solar cells, reduction of Rs is one effective means to improve the performance of the device. It is reported that if the series resistance increases per 0.1Ω, the FF of an inorganic solar cell declines about 2.5% [10]. Generally, it considers the probe resistance is about 10Ω, and the resistance of the electrodes is in the range of 4–15Ω, the two resistance can be omitted when the device area (A) is smaller than 0.01 cm^2[11-12]. And if the contacts between the electrodes and the active layer are Ohmic contacts and there are no large barriers at the interfaces between the organic layers in the device, the contact resistances can be negligible, too. Then the dominating contribution to the Rs is caused by the large resistivity of the organic layers. Here we can give a rough estimate of the resistivity according to equation (4)

$$\rho = \frac{1}{\sigma} = \frac{1}{nq\mu} \quad \textbf{(4)}$$

Here, ρ is resistivity, σ is conductivity, n is the density of free carriers in organic films, q is the elementary charge and μ is carrier mobility.

Taking the typical values in organic solar cells here, n is about $10^{17}cm^{-3}$, μ is about $10^{-3}cm^2V^{-1}s^{-1}$, so the calculated ρ about $10^5\Omega$ cm. If the film thickness of the active layer is 100 nm, then the resistance of the active layer is R=1Ω cm^2. There are reports that by improving the mobility of carriers, Rs can be reduced and the efficiency of the devices is enhanced significantly [12]. And if the mobility is fixed, larger film thickness will lead to larger Rs [13].

5.2.2 Shunt Resistance(R_{sh}):

Shunt resistance denotes the current losses in the cells, such as the current leakage from the edge of the cell, current leakage from the pinholes in the film or the current leakage by the traps. It has the effect of dividing the current in the equivalent circuit. Ideal Rsh should approach infinity, so current flows through Rsh is zero, i.e. there is no current leakage in the device. If Rsh is small, the current flowing through it cannot be neglected. Moreover, the current will change with the applied voltage, which makes the J–V curve deviate from ‘‘square’’ and thus lead to a lower FF.

When the layer thickness of the blend increases, the J_{SC} of the device was improved because of more light absorption in a thicker film. However, the Rsh of the device decreased which in turn decreased FF. In thick films, the charges need to travel a long distance before being collected by the electrodes, when the transit time is longer than the lifetime of the carriers, recombination will happen and lead to lower J_{SC} and larger R_{sh} [14]. If the device is annealed thermally, the interfacial morphology can be improved. The researchers found that R_s of the devices with and without thermal annealing are almost the same, while R_{sh} increased a lot after annealing. So the conclusion is that a good interfacial morphology can prevent current leakage and surface recombination.

5.2.3 Diode:

It was already defined in chapter 1 that Region II of the J–V curve is limited by the diode, the property of which can be characterized by equation (5). At room temperature there are only two variables in equation (5) n and J_s. n is dominated by the exciton dissociation and recombination in the device, and J_S is reported to be related to the difference between the highest occupied molecular orbital (HOMO) level of the donor material and the lowest unoccupied molecular orbital (LUMO) level of the acceptor material.

$$J = J_S[\exp(qV/nk_BT) - 1] \quad \textbf{(5)}$$

5.3 Summary:

Based on the three equivalent circuit elements, namely Rs, Rsh and diode, we reviewed the present understanding on influence of these parameters on device. Rs has a pronounced effect on the shape of J–V curve around V_{OC}, large Rs can divide the voltage from the diode, leading to a slower rise of J with increasing positive V, i.e., the J–V curve becomes less ‘‘square’’ and FF decreases. Rsh governs the shape of the J–V curve around J_{SC} , small R_{sh} divides the current from Jph, leading to J increasing with the reverse bias, i.e., the J–V curve becomes less ‘‘square’’ and FF decreases as well. The properties of the diode determine the curvature of the J–V curve around the maximum power point.

5.4 References:

[1] G. L. Araujo, E. Sanchez, and M. Marti, Sol. Cells5, 199 **(1982).**

[2] K. Nishioka, N. Sakitani, Y. Uraoka, and T. Fuyuki, *Sol. Energy Mater. Sol.Cells*91, 1222 **(2007).**

[3] B. Mazhari, *Sol. Energy Mater*. Sol.Cells 90, 1021 **(2006).**

[4] National Instruments. Part ii - photovoltaic cell i-v characterization theory and lab view analysis code. Development Zone, URL:http://zone.ni.com/devzone/cda/tut/p/id/7230.

[5] C. Waldauf, M. C. Scharber, P. Schilinsky, J. A. Hauch and C. J. Brabec,*J. Appl. Phys.*, **2006**, 99, 104503

[6] G. Li, et al., "High-efficiency solution process able polymer photovoltaic cells by self-organization of polymer blends," *Nature Materials*, vol. 4, pp. 864-868, **Nov 2005**.

[7] F. Shirland, "The history, design, fabrication and performance of CdS thin film solar cells," *Advanced Energy Conversion*, vol. 6, pp. 201-202, **1966.**

[8] U. Rau, P. O. Grabitz and J. H. Werner, *Appl. Phys. Lett.*,**2004**,85, 6010.

[9] J. Xue, S. Uchida, B. P. Rand and S. R. Forrest,*Appl. Phys. Lett***., 2004,** 84, 3013.

[10] R. A. Street, K. W. Song and S. Cowan, *Org. Electron.*, **2011,** 12, 244.

[11] Boyuan Qi ab and Jizheng Wang, *Phy chem. Chem. Phy*. **2013,** 15, 8972

[12] Y. Zhang, J. Yu, J. Huang, R. Jiang and G. Huang,*J. Phys. D: Appl. Phys.*, **2012**, 45, 175101

[13] Y. Shen, K. Li, N. Majumdar, J. C. Campbell and M. C. Gupta,*Sol. Energy Mater. Sol. Cells*, **2011,** 95, 2314.

[14] M. Lenes, L. J. A. Koster, V. D. Mihailetchi and P. W. M. Blom, *Appl. Phys. Lett.*, **2006,** 88, 243502.

CHAPTER 6

RESULTS AND DISCUSSIONS

6.1 Study of Conventional Devices:

It is very much important to analyze the device parameters of the organic solar cells in view to improve their efficiency and lifetime in inverted as well as conventional organic solar cells. Hence, herein, we will analyze the inverted as well as conventional geometries using different kind of interface layer, active layer material etc. First of all we will show the device parameters for the device structure ITO|PEDOT:PSS|P3HT:PC60BM|Al (Figure 6.1-6.3) whose device parameters are listed in Table 6.1

6.1.1 Conventional organic solar cell devices based on PEDOT: PSS as the hole transport layer

The device data is presented in Table 6.1. J-V measurements have been carried out and result is represented in Figure 6.1.

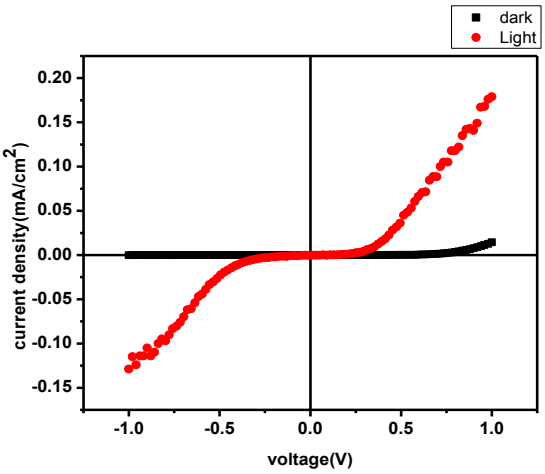

Figure6.1: J-V plot of PEDOT: PSS in solar cell with device structure ITO|PEDOT:PSS|P3HT:PC_{60}BM|Al

Table 6.1 Device Parameters of ITO|PEDOT:PSS|P3HT:PC60BM|Al(S-factor)

Rotation speed (rpm)	**Voc (V)**	**Jsc (mA/cm^2)**	**FF (%)**	**Rs ($\Omega\ cm^2$)**	**Rsh ($k\Omega\ cm^2$)**
2000	0.11	0.0053	50	50	0.123

As obvious from the Table 6.1 the device based on PEDOT: PSS shows Voc ≈ 0.11V, Jsc ≈ 0.0053mA/cm^2, Fill factor (FF) ≈ 50%, Rs ≈ 50Ω cm^2, Rsh ≈ 0.123 kΩ cm^2. The device shows very poor performance in view of Voc, Jsc and FF. This may be due to being S-shape of the J-V characteristics. This shape of the J-V plot may be originally due to different effects e.g. unbalance of charge carrier mobilities, defects or dipoles at the interface, energy barriers and low surface recombination rate of the cathode, etc. However, more observation or measurements are need to know the exact cause of S-shape. Further, the series as well as shunt resistance support the poor performance of the PEDOT: PSS based device as it show very low shunt resistance and very high series resistance [1].

Further, we done more experiments and improved the device performance of the PEDOT: PSS based device whose J-V characteristics are shown in Figure 6.2 and Figure 6.3 and the device parameters are listed here in Table 6.2. Now these device show better results in view of their Jsc, Voc, FF and hence lower value of series resistance and high value of shunt resistance as expected.

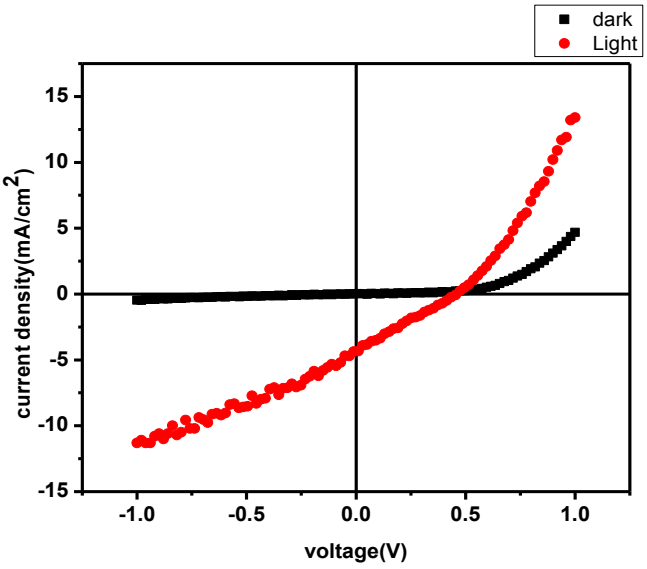

Figure 6.2: J-V plot of PEDOT: PSS (before annealing) in solar cell with device structure ITO|PEDOT:PSS|P3HT:PC60BM|Al

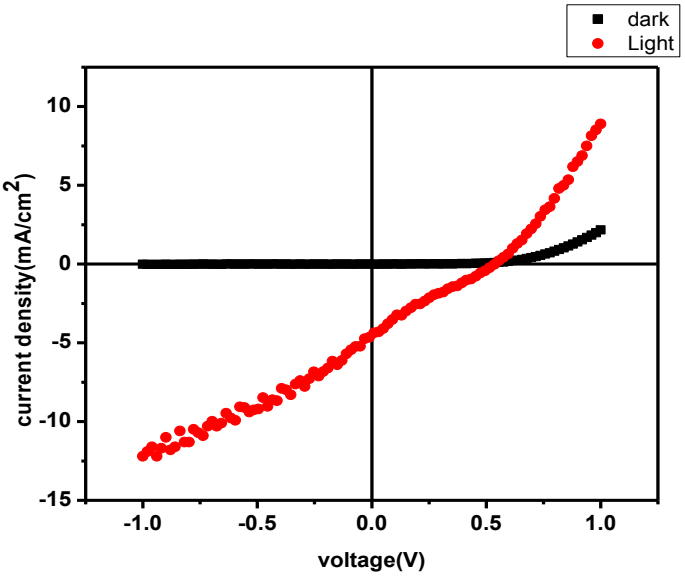

Figure 6.3: J-V plot of PEDOT: PSS (after annealing) in solar cell with device structure ITO|PEDOT:PSS|P3HT:PC60BM|Al

Table 6.2 Device Parameters of ITO|PEDOT:PSS|P3HT:PC60BM|Al

Figure No.	**Rotation speed(rpm)**	**Voc (V)**	**Jsc (mA/cm^2)**	**FF (%)**	**PCE (%)**	**Rs ($\Omega\ cm^2$)**	**Rsh ($k\Omega\ cm^2$)**
6.1	2000	0.475	4.34	23.2	0.479	35.73	162
6.2	2000	0.550	4.37	23.1	0.561	56.33	150

However, long term stability is still a concern because of its acidic and hygroscopic nature of PEDOT: PSS [2]. Moreover, with its low work function of around 5.1eV, PEDOT: PSS can cause energy-level mismatch with high work function. Hence, we were motivated to replace PEDOT: PSS with alternative materials such as- MoO_3, NiO and V_2O_5.

One of the major aspects of designing efficient organic solar cells (OSCs) is the engineering of interfacial carrier transport layers between organic layer and metallic electrodes. Among various materials available for interfacial layers, transition metal oxides such as- MoO_3, NiO and V_2O_5, have great potentials owing to the following:

- Wide range of energy level aligning capabilities.
- Formation of low resistance ohmic contact by these oxides.
- High transparency and desirable band structure.
- Excellent ambient stability in ambient environment which can extend the lifetime of organic electronics.

The above factors, energy level compatibility (see Figure 6.4), low cost and high throughput production using solution route as well as evaporation route makes MoO_3 as the most attractive alternative to PEDOT: PSS.

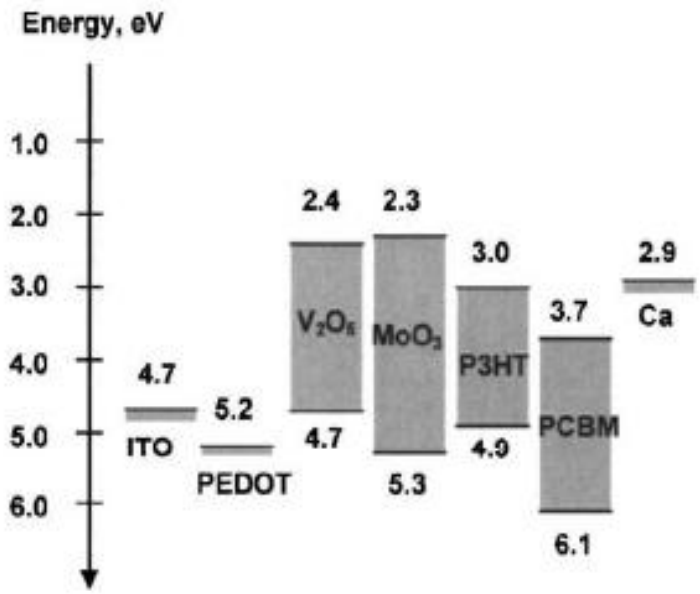

Figure 6.4: Schematic comparing the energy levels of various layers used in OPVs [3]

6.1.2 Replacing PEDOT: PSS with MoO3 (synthesized through solution route):

Herein, we analyze the device structure of ITO|MoO_3|P3HT:PC60BM|Al. Firstly, MoO_3 interfacing layer synthesized through solution route whose J-V characteristics is shown in Figure 6.5 and Figure 6.6 and device parameters are listed in Table 6.3.As obvious from the table 6.3, the device based on MoO_3 (solution route) shows Voc ≈ 0.15V, Jsc ≈ 0.368mA/cm^2, Fill factor (FF) ≈ 21.4%, PCE ≈ 0.02%, Rs ≈ 62.7 Ω cm^2, Rsh ≈ 0.231 kΩ cm^2.

The device parameters were not upto the mark as expected. This may be due to surface roughness of the film [2] and MoO3 nanoparticles may agglomerate and may not give uniform surface morphology before annealing. This may increase the roughness of the film which may lead to leakage current. Further AFM study is needed to clarify and establish this concept. However, other observations and measurement are also needed to know the exact cause such as X-ray photoemission spectroscopy to further investigate the surface characteristics of the MoO_3.

Further, we done more experiments and improved the device performance of the MoO3 based device synthesized through evaporation route whose J-V characteristics as shown in Figure 6.6 and the device parameters are listed in Table 6.4. Now this device shows better results in view of their Jsc, Voc, FF (Fill factor) and hence lowers value of series resistance (Rs) and high value of shunt resistance (Rsh).

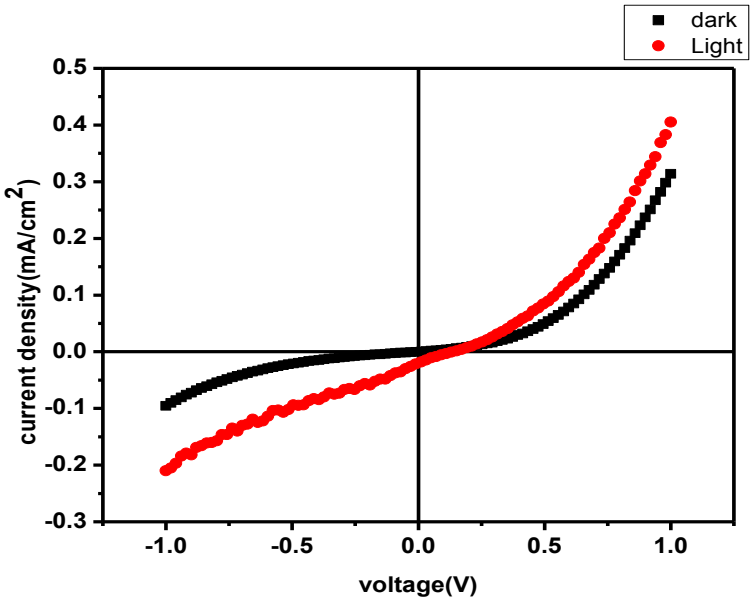

Figure 6.5 J-V plot for solar cell with device structure

ITO|MoO3|P3HT:PC60BM|Al

Table 6.3 Device parameters of ITO|MoO3|P3HT:PC60BM|Al

Voc **(V)**	**Jsc** **(mA/cm^2)**	**FF** **(%)**	**PCE** **(%)**	**Rs** **(Ω cm^2)**	**Rsh** **(kΩ cm^2)**
0.15	0.368	21.4	0.02	62.7	0.231

6.1.3 Replacing PEDOT: PSS with MoO3 (synthesized through evaporation route):

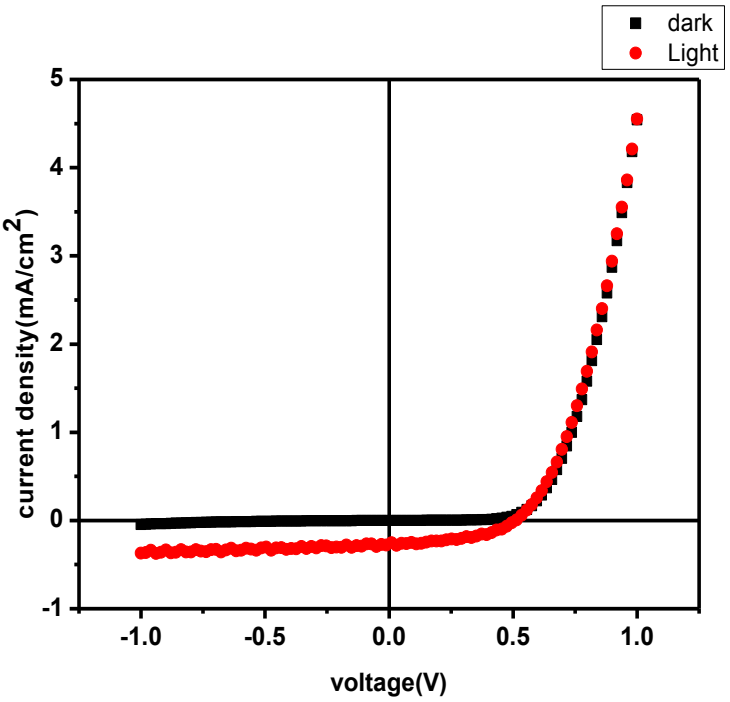

Figure 6.6 J-V plot for solar cell with device structure

ITO|MoO_3|P3HT:PC60BM|Al

Table 6.4 Device parameters of ITO|MoO_3|P3HT:PC60BM|Al

Voc (V)	**Jsc (mA/cm^2)**	**FF (%)**	**PCE (%)**	**Rs ($\Omega\ cm^2$)**	**Rsh ($k\Omega\ cm^2$)**
0.51	2.54	49	0.65	6.75	0.255

The different parameters of the device ITO|MoO_3|P3HT:PCBM|Al is listed in Table 6.4.In this device structure MoO_3 is synthesized through evaporation route using thermal evaporator. Using this MoO_3 HTL the solar cell showed a fill factor (FF) of 49%. The VOC and JSC values were 0.51V and 2.54mA/cm^2 respectively. The power conversion efficiency (PCE) value obtained is

0.65%. The series resistance and shunt resistance value obtained is 6.75Ω cm^2 and 0.255kΩ cm^2 respectively. The evaporation route MoO_3 based device shows better performance in terms of device parameters may be due to better film formation ability of evaporation route. Thus, MoO_3 has the potential to be a good replacement for PEDOT: PSS. Further optimization of the film is required to obtain better device efficiency.

Apart from the conventional devices based on MoO3 and PEDOT: PSS, we also analyzed the different devices parameters of inverted structure of the devices based on solution process ZnO as well as ZnO-PDADMAC based nanocomposites. Their J-V characteristics and device parameters are discussed in next section.

6.2 Study of Inverted Devices:

In case of inverted devices we have used the following general structure:

ITO|Interface Layer|Active Layer|MoO3|Al

For our investigation we chose the following device structure:

ITO|ZnO|P3HT:PCBM|MoO3|Al

ZnO is good choice because of its environmental stability, relatively high electron mobility and optical transmittance [4] and its wide and direct band gap (3.37 eV) (Figure 6.7).

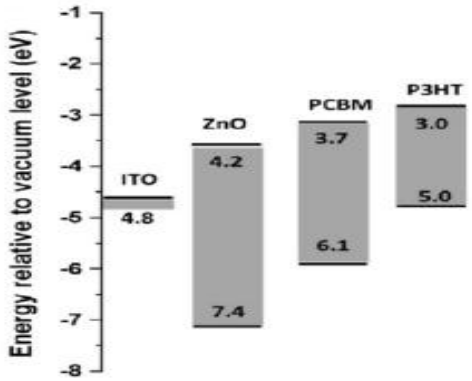

Figure 6.7 Energy level diagram showing ZnO with other materials used [5].

6.2.1 Using ZnO as ETL:

ZnO film prepared by solution process is used here. 0.235 g of zinc acetate dihydrate was added in 5 ml propanol and allowed to stir for 5 min. A white cloudy solution is obtained here. Now after 5 minutes, few drops of DEA are added to this solution. Slowly we will observe that the cloudiness disappears and a colourless and transparent solution is obtained. Now, this solution is allowed to stir at 60°C for 2 hours. The solution is then kept untouched and undisturbed for 24 hours. After coating this solution on ITO at 2000 rpm, the substrate should be heated at 200°C for 30 minutes. The active layer tried out with ZnO is P3HT:PC60BM.

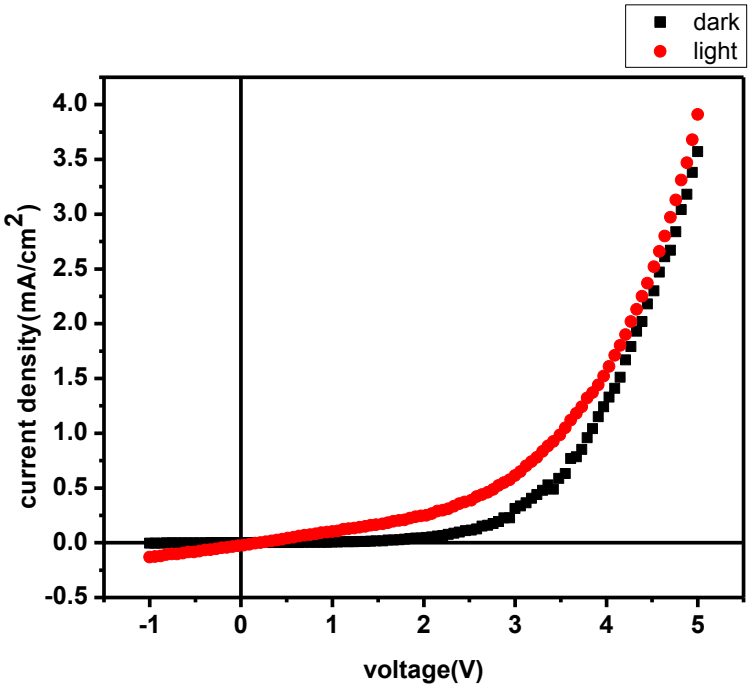

Figure 6.8 J-V plot for solar cell with device structure

ITO|ZnO (0.1g) |P3HT:PC60BM|MoO3|Al

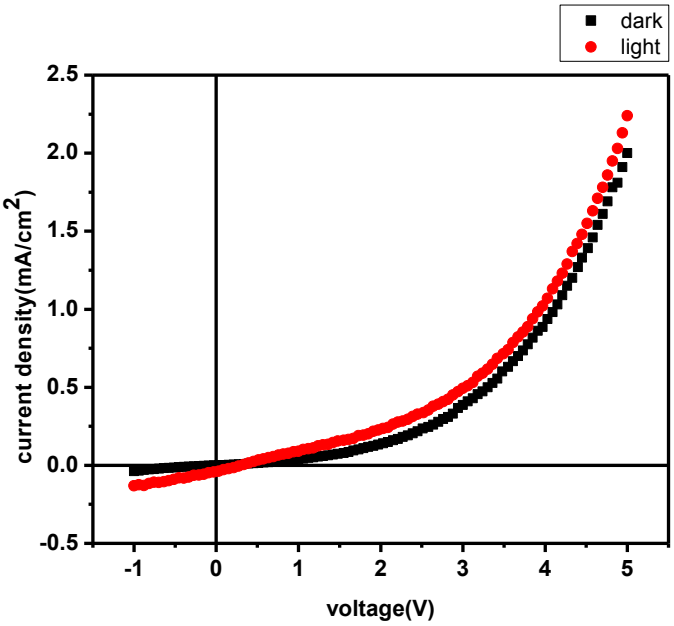

Figure 6.9 J-V plot for solar cell with device structure

ITO|ZnO (0.135g) |P3HT:PC60BM|MoO3|Al

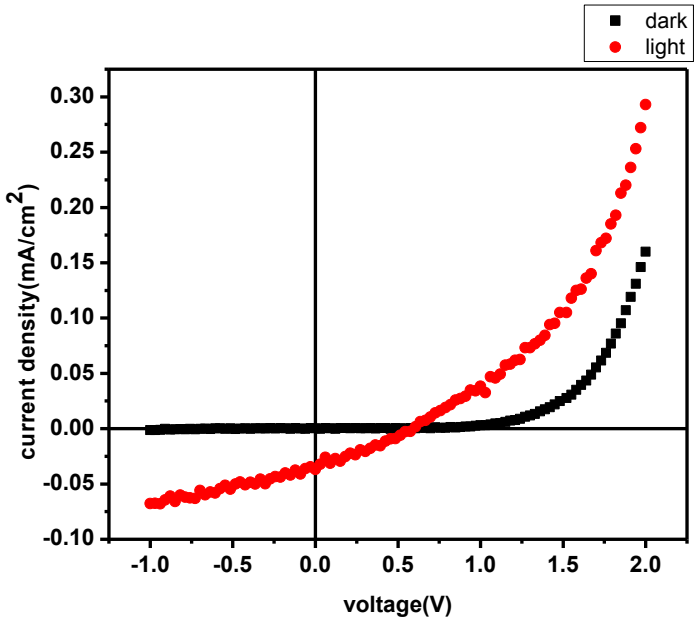

Figure 6.10 J-V plot for solar cell with device structure

ITO|ZnO (0.235g) |P3HT:PC60BM|MoO3|Al

Table 6.3 Device parameters of ITO|ZnO|P3HT:PC60BM|MoO3|Al

Concentration (g)	**Voc (V)**	**Jsc (mA/cm2)**	**FF (%)**	**PCE (%)**	**Rs (Ω cm2)**	**Rsh (kΩ cm2)**
0.10	0.213	0.546	28.0	0.03	17.00	0.387
0.135	0.33	0.938	25.7	0.08	29.50	0.523
0.235	0.60	0.100	28.0	0.15	89.10	11.37

It is clear from Table 6.3 that the device ITO|ZnO|P3HT:PCBM|Al has given the best device parameters for the concentration of 2wt% of ZnO. In each case the ZnO layer has been spin coated at 3500 rpm. As we lower the concentration of ZnO, the performance of the solar cell decreases. Shunt resistance value obtained for the concentration of 2wt% is drastically increased which improve the device performance. However, still more studies such as AFM are needed to confirm which concentration of ZnO gives better film as well as better device performance.

As seen in Figure 6.8, the solar cell shows almost negligible shunt resistance and low fill factor (FF). Also, downside is the current density values. They are very low. We have tried to increase it as mentioned before by using ZnO-polymer composite films as the electron transport layer (ETL). We will see that current density values increase exponentially due to the composite films used. A possible reason for low current density values maybe the defects created in ZnO film during heat treatment and due to the low spatial distribution of ZnO nanoparticles. Hence, we started thinking about making a composite of ZnO solution with cationic poly-electrolytes and chosen the well-known polymer PDADMAC.

In pure ZnO film the ZnO nanoclusters have non-homogenous arrangement and no proper connectivity exists between the nanoclusters (Figure 6.11 (a)). On addition of the polymer, the clusters arrange into homogenous manner and the polymer strands bind the clusters together thus providing a suitable connecting path in between the nanoclusters (Figure 6.11 (b)). After addition of the polymer and spin coating it, the film needs to be heated at 200°C for 30 minutes.

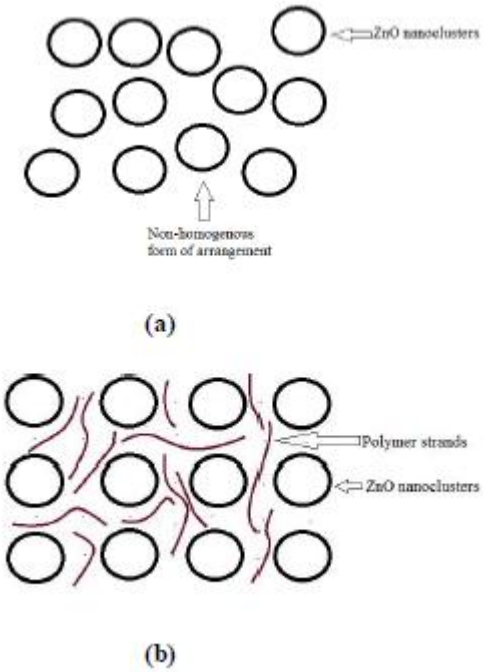

Figure 6.11 Arrangement of ZnO nanoclusters **(a)** before addition of polymer and **(b)** after addition of polymer and heating.

6.2.2 Use of ZnO-PDADMAC nanocomposite layer:

This nanocomposite layer was prepared using solution process. To make PDADMAC solution we added 0.5 ml PDADMAC in 0.5 ml of water. This solution was stirred for 30 minutes. Now to prepare the nanocomposite solution, this 1 ml PDADMAC solution was added in 2 ml of ZnO solution. Also after a 5 minute interval, 2 to 3 drops of DEA were added in this solution and the resultant mixture was then stirred for 30 minutes.

PDADMAC is a cationic polyelectrolyte [6] which is widely used as a model for charged polymers behaviour and also in various industrial applications [7,8]. Using this polymer gave us positive results (Figure 5.11).

Using active layer- P3HT:PC60BM

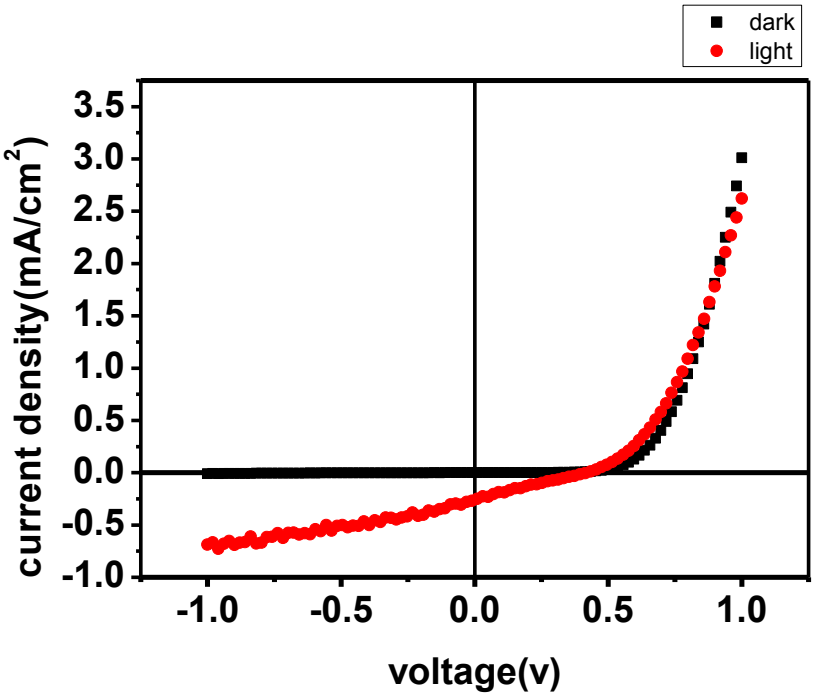

Figure 6.12 J-V plot for for solar cell with device structure ITO|ZnO-PDADMAC|P3HT:PC60BM|MoO3|Al

Table 6.4 Device parameters of ITO|ZnO-PDADMAC|P3HT:PC60BM|MoO3|Al

Voc (V)	**Jsc (mA/cm2)**	**FF (%)**	**PCE (%)**	**Rs (Ω cm^2)**	**Rsh (kΩ cm^2)**
0.434	2.49	24	0.26	13.8	0.545

The different parameters of the device ITO|Zno-PDADMAC|P3HT:PCBM|Al is listed in Table 6.4. Using this ZnO-PDADMAC ETL the solar cell showed a fill factor (FF) of 26%. The VOC and JSC values were 0.434V and 2.49mA/cm^2 respectively. The series resistance and shunt resistance value obtained is 13.8Ω cm2 and 0.545kΩ cm2 respectively. As shown in Table6.4, the device parameters of ZnO-PDADMAC improves as compare to pristine ZnO. Herein we obtain a Rs≈13.8 which is low to Rs≈89.10, when ZnO pristine used as a interfacing layer.

Further, Voc, Jsc and FF also improved as compare to pristine ZnO interfacing layer. This may be due to the uniformity of the interfacing layer when PDADMAC polymer is used with ZnO. This, observation is in the streamlined of our observation of smooth surface of ZnO-PDADMAC nanocomposites as published in Applied physics. However, this device needs further examination by optimization of the thickness of buffer layer with the help of profilometry characterization technique as working principle already explained in chapter 4.

Table 6.5 Profilometry results using ZnO-PDADMAC interfacing layer

Rpm speed	**Thickness of layer (nm)**	**Rpm speed**	**Thickness of layer(nm)**
4500	260	7500	35
3500	360	6500	83
2500	490	5500	217

To make the sample for profilometry the interfacing layer (Zno-PDADMAC) is spin coated on the glass sheet at different Rpm and then annealed at 200^{o}C for 15 minutes.

As shown in Table 6.5 as we increase the Rpm of the spin coated interfacing layer the thickness of the layer decreases which decreases the series and shunt resistance effect. However, this device needs further investigation and formation of the device structure at different Rpm to find out the device parameters of the device.

6.2.3 Using PFN as ETL:

To improve the device performance we are further motivated to replace ZnO with PFN layer. Herein, a J-V characteristic is shown in figure 6.13 and the device parameters are tabulated in Table 6.5.

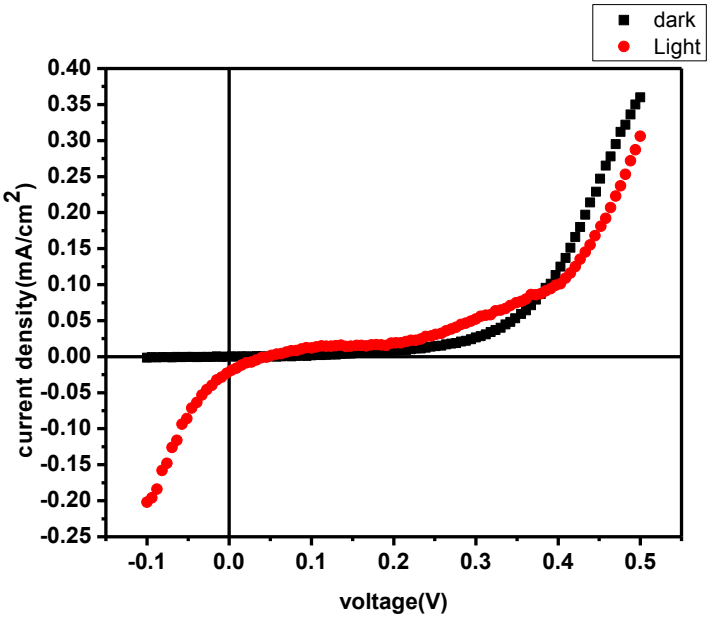

Figure 6.13 J-V plot for for solar cell with device structure

ITO|PFN|P3HT:PC60BM|MoO3|Al

Table 6.5 Device parameters of ITO|PFN|P3HT:PC60BM|MoO3|Al

Voc **(V)**	**Jsc** **(mA/cm^2)**	**Rs** **(Ω cm^2)**	**Rsh** **(kΩ cm^2)**
0.514	0.05	1602.2	1.74

The different parameters of the device ITO|PFN|P3HT:PCBM|Al is listed in Table 6.5. Using this PFN ETL the solar cell showed a values of series resistance and shunt resistance of 1.60kΩ cm^2 and 1.74kΩ cm^2 respectively. The Voc and Jsc values were 0.514V and 0.05mA/cm^2

respectively. The series resistance value obtained is very high which may reduce the current density to a very low value. However, this needs further investigation using AFM to know the exact reason to this high value of series resistance.

Apart from above said device fabrications I was also involve into a study of morphological observations of ZnO-PDADMAC layer through SEM and PL studies which will be discussed in next section of the same chapter.

6.3 SEM(Scanning electron microscope) Analysis:

The scanning electron microscope (SEM) is a powerful and frequently used instrument, in both academia and industry, to study, for example, surface topography, composition, crystallography and properties on a local scale

The Figs. 6.14(c) and 6.14(d) clearly show the agglomerated ZnO nanoparticles when its spin coated on ITO from the solution. Herein, we want to make it clear that most of the devices with pristine ZnO as interface layer are highly susceptible for shorts in our experimental conditions. We tried to make the device using pristine ZnO by varying composition from 0.035 to 0.535 g/5 ml. However, we came to an end of shorting of the devices, and only a few worked with lower values of efficiency. The devices with the composite layers produced good device as shown in Table6.4. We know that device efficiency using pristine ZnO as an interface layer is small. Further, optimization of solution concentration/thickness may give better performance as reported in literature for pristine ZnO based inverted devices. However, here our motive is the demonstration of effect of ZnO-polyelectrolyte nanocomposite on the device performance. These values (Table6.4) of device parameters showed superior interface properties of the ZnO-PDADMAC nanocomposite. The Figs.6.14(a), 6.14(b), 6.14(a), and6.14(b) show a representative SEM image of the spin coated nanocomposite of ZnO-PDADMAC on the ITO, which clearly demonstrates that the ZnO nanoparticles are finely distributed over the entire surface and the surface is very smooth (Fig.6.14)

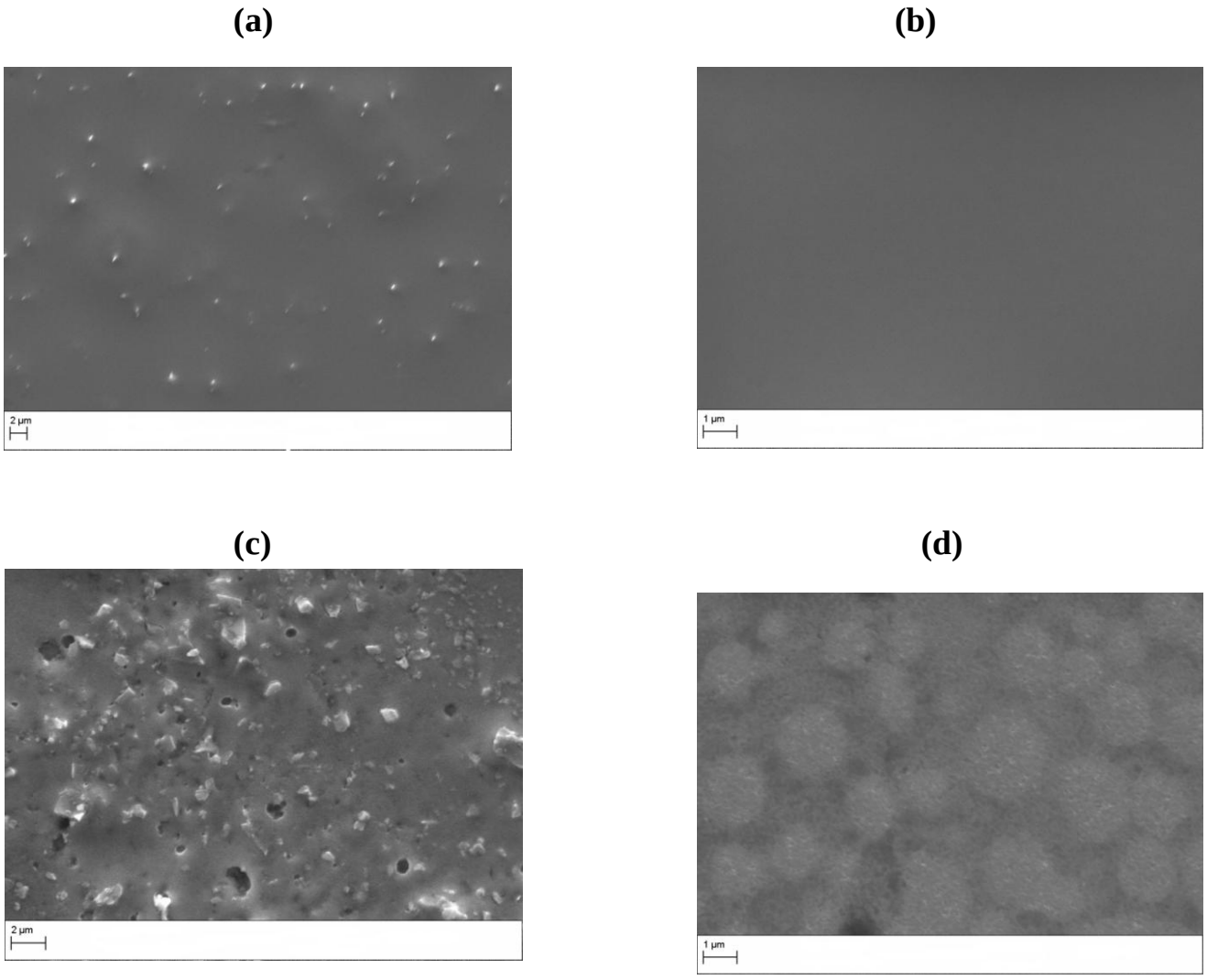

Figure 6.14. SEM of a film of (a) and (b) ZnO-PDADMAC, (c) and (d) pristine zinc oxide, showing agglomerated zinc oxide nanoparticles in (c) and (d), and finely distributed and planar red ZnO-PDADMAC nanocomposite film**.**

6.4 Photoluminescence (PL) analysis:

PL spectroscopy gives information on low lying energy levels of the valence band. During the experiment the excitation provided by laser is much larger than the band gap of the material. The photo excited charge carriers- electrons and holes relax in their respective bands and recombine to give emission of photon. The samples were prepared in chlorobenzene as solvent and the measurements were carried out at room temperature. The PL signal was detected with Perkin Elmer LF55 having Xenon spectrophotometer.

In order to explain the improved current collection in devices with composite layer, we tried to investigate the effect of PDADMAC, PVP, and PSS modification on the surface defects of Zn nanoparticles through PL under 330 nm photo excitation as shown in Figure 6.15. We observe only pristine ZnO and ZnO-PDADMAC .The emission band at ≈ 370 nm may be due to exciton emission. The two shoulders at ≈ 420 and ≈ 439 nm may be originating from the Zn interstitial defects. Further, the broad emission at ≈ 475 nm may be attributed to transition among photo excited carriers, oxygen vacancies, surface defects, etc. As obvious from Figure 6.15 the emission intensity decreases for composite layer with respect to the pristine zinc oxide layer, which may be indication of passivation of surface traps in composite layers.

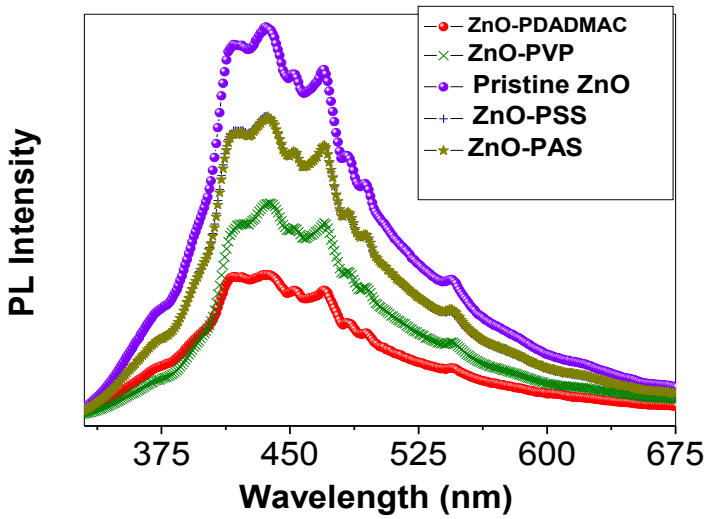

Figure 6.15 PL spectra of ZnO, ZnO-PSS, ZnO-PAS, ZnO-PVP, and ZnO-PDADMAC films prepared through spin coating at 3500 rpm

6.5 References:

[1] Boyuan Qiab and Jizheng Wang ,Fill factor in organic solar cells *Phys. Chem. Chem. Phys.*,**2013**,15, 8972.

[2] Seiichiro Murase and Yang Yang, Solution Processed MoO3 interfacial layer for Organic photovoltaics,*Adv. Material* **2012** ,24, 2459-2462.

[3] Vishal Shrotriya, Gang Li, Yan Yao, Chih-Wei Chu, and Yang Yang, *Appl. Phys. Lett.*, **2006**, 88, 073508.

[4] Youssef Jouanea, Silviu Colis, Guy Schmerber, Aziz Dinia, Patrick Lévêque, Thomas Heiser, Yves-André Chapuis ;Influence of flexible substrates on inverted organic solar cells using sputtered ZnO as cathode interfacial layer, *organic electronics* 14(**2013**) 1861-1868

[5] Mohammed Aziz Ibrahema, Hung-Yu Wei, , Meng-Hung Tsai, , Kuo-Chuan Ho, Jing-Jong Shyue, , Chih Wie Chu, Solution-processed zinc oxide nanoparticles as interlayer materials for inverted organic solar cells, *Solar Energy Materials and Solar Cells*, **2013**, 108, 156.

[6] Gema Marcelo, M. Pilar Tarazona, Enrique Saiz, *Elsevier Polymer*, **2005**, 46(8), 2584.

[7] Dautzenberg H, Go¨rnitz E, Jaeger W., *Macromol Chem Phys* Ed, **1998**,199, 1561.

[8] Matsumoto A., *Prog Polymer Science*, **2001**, 26, 189.

CHAPTER 7

CONCLUSION

In our investigation of organic solar cell we studied both conventional as well as inverted devices. The device structures investigated here are:

(1) ITO|PEDOT:PSS|P3HT:PC60BM|Al

(2) ITO|MoO_3|P3HT:PC60BM|Al

(3) ITO|ZnO|P3HT:PC60BM|MoO_3|Al

(4) ITO|ZnO-PDADMAC|P3HT:PC60BM|MoO_3|Al

(5) ITO|PFN|P3HT:PC60BM|MoO_3|Al

The device parameter of structure(1) shows series resistance of 35.73Ω cm^2 and shunt resistance of 0.162 kΩ cm^2 and also it shows a high current density of 4.34 mA/cm^2 While the device parameters of structure(2) shows series resistance of 6.75Ω cm^2 and shunt resistance of 0.255kΩ cm^2. The device parameter of MoO_3 based device shows improved series resistance Rs ≈ 4 times better than PEDOT:PSS and shunt resistance obtained was approximately same.

Now, we analyze the device parameter of structure(3). We varied the concentration of pristine ZnO from 0.10-0.235gm and obtained superior results at 0.235gm concentration as compare to other cocentration. The device parameter shows at 2%wt concentration are Rs ≈ 89.10Ω cm^2 and Rsh ≈ 11.37 kΩ cm^2 while Voc and Jsc are 0.60V and 0.100mA/cm^2 respectively. The high value of shunt resistance shows better open circuit voltage while due to high series resistance the low current density was obtained.

Now we show the effect of series resistance and shunt resistance on other device parameters such as Voc, Jsc and FF(Fill factor) with the help of Table 7.1

Table 7.1 Device parameters of conventional and inverted organic solar cells

Device structure	**Voc (V)**	**Jsc (mA/cm^2)**	**FF (%)**	**PCE (%)**	**Rs ($\Omega\ cm^2$)**	**Rsh ($k\Omega\ cm^2$)**
PEDOT: PSS	0.475	4.34	23.2	0.479	35.73	0.162
MoO3 (Sol.)	0.15	0.368	21.4	0.02	62.7	0.231
MoO3 (Evap.)	0.51	2.54	49	0.65	6.75	0.255
ZnO (0.235g)	0.60	0.100	28	0.15	89.10	11.75
ZnO-PDADMAC	0.434	2.49	24	0.26	13.8	0.545
PFN	0.514	0.05	-	-	1602.2	1.74

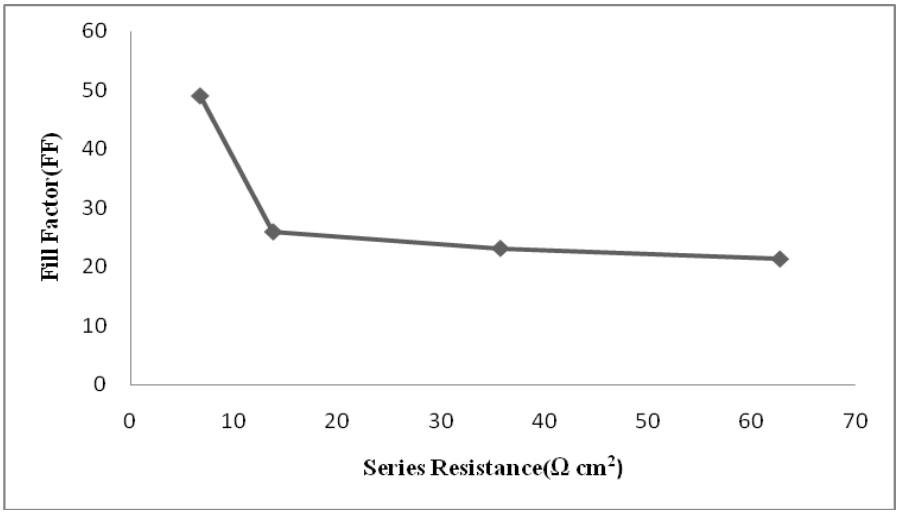

Figure 7.1 Graph between Fill factor and Series resistance of different device structure

We ploted graph between series resistance and Fill factor. It shows that the fill factor decreases when series resistance increases. Fill factor is high in MoO3 based structure i.e. 49% when series resistance(Rs) ≈ 6.75Ω cm^2. On the other hand, Fill factor is low in case of MoO_3(Solution route) i.e. 21.4% when Rs ≈ 62.7Ω cm^2. This shows that series resistance affects fill factor. Again we plotted Voc Vs Rsh for device and result is shown in Figure 7.2.

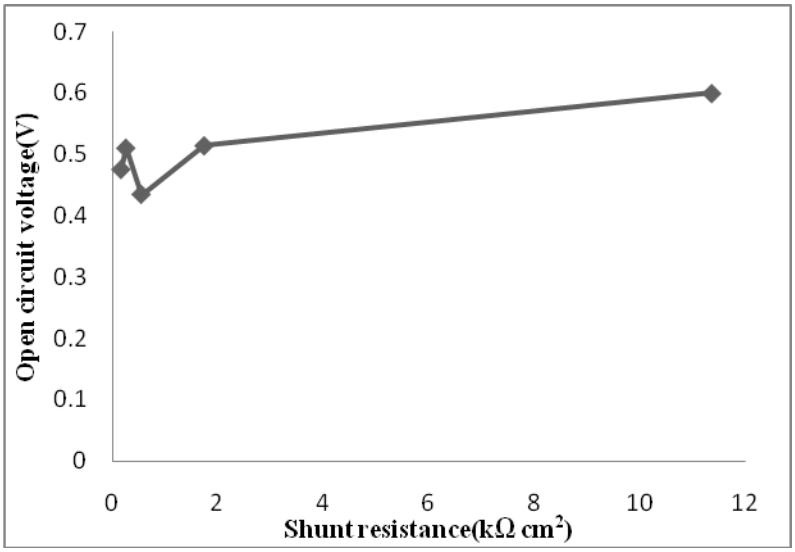

Figure 7.2 Graph between Open circuit voltage and Shunt resistance of different device structure

This graph shows that the shunt resistance affects the open circuit voltage. As shunt resistance increases open circuit voltage also improves with that. We get high shunt resistance(Rsh) ≈ 11.37kΩ cm^2 corresponding to the Voc ≈ 0.60V which is highest among all.

Further, we plotted Jsc Vs Rsh and result is shown in Figure 7.3

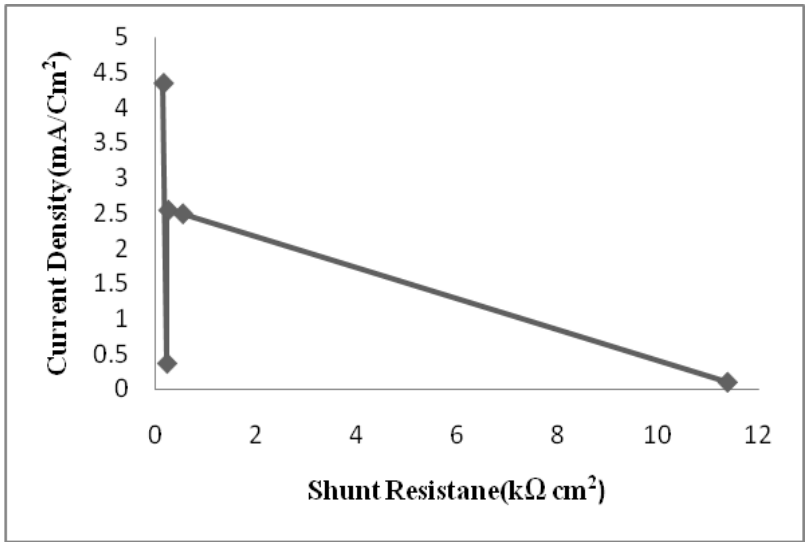

Figure 7.3 Graph between Current Density and Shunt resistance of different device structure

This graph shows the relation between shunt Resistance and Current Density. However, we are not able to get any useful information and correlation between the device parameters. Hence, it needs further investigation and observations to find out the effect of shunt resistance and series resistance on current density.

Moreover, the Figure7.4 shows a relation between Fill factor and shunt resistance

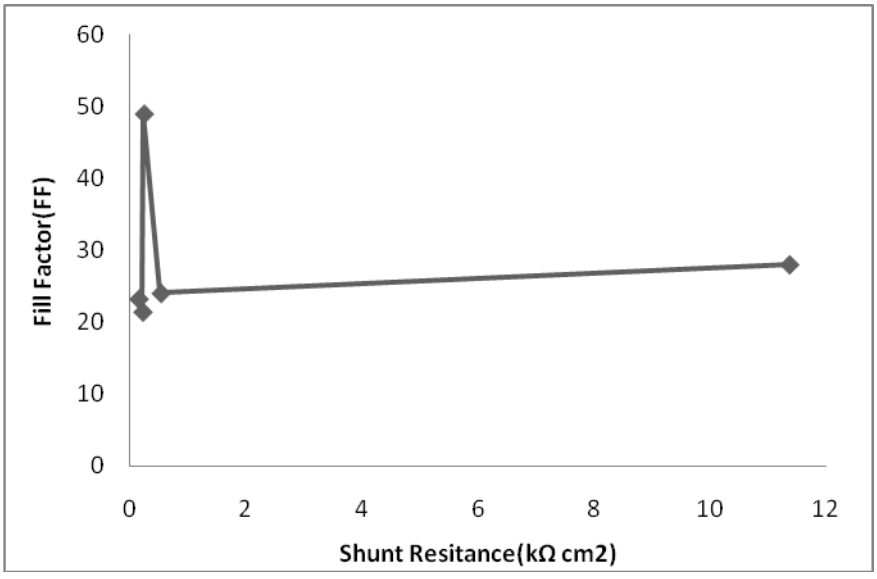

Figure 7.4 Graph between Fill factor and Shunt resistance of different device structure

It shows that when shunt resistance value is low, it affects the fill factor, but if its value becomes high, its affects on fill factor becomes neglicible and not varied much at high value of shunt resistance. Further we need more observatios and measurements to come into final conclusion regarding the affect the shunt resistance on fill factor.